INL/JOU-23-72708-Revision-0

RELAP5-3D Validation Studies based on the High Temperature Test Facility

June 2024

Robert Forrester Kile, Aaron S Epiney, Nicholas R. Brown

Changing the World's Energy Future

Idaho National Laboratory

INL is a U.S. Department of Energy National Laboratory operated by Battelle Energy Alliance, LLC

INL/JOU-23-72708-Revision-0

RELAP5-3D Validation Studies based on the High Temperature Test Facility

Robert Forrester Kile, Aaron S Epiney, Nicholas R. Brown

June 2024

Idaho National Laboratory
Idaho Falls, Idaho 83415

http://www.inl.gov

Prepared for the
U.S. Department of Energy
Under DOE Idaho Operations Office
Contract DE-AC07-05ID14517

RELAP5-3D Validation Studies based on the High-Temperature Test Facility

Robert F. Kile[1,2], Aaron S. Epiney[2], Nicholas R. Brown[1]
[1]University of Tennessee, Knoxville, Tennessee, USA
[2]Idaho National Laboratory, Idaho Falls, Idaho, USA
Keywords: Gas-cooled reactor, thermal hydraulics, benchmark, reactor safety, HTTF, validation, RELAP5-3D

Abstract
In the spring and summer of 2019, experiments were conducted at the High-Temperature Test Facility (HTTF) that form the basis of an upcoming high-temperature gas-cooled reactor (HTGR) thermal hydraulics (T/H) benchmark. HTTF is an integral effects test facility for HTGR T/H modeling validation. This paper presents RELAP5-3D models of two of those experiments: PG-27, a pressurized conduction cooldown (PCC); and PG-29, a depressurized conduction cooldown (DCC). These models used the RELAP5-3D model of HTTF originally developed by Paul Bayless as a starting point. The sensitivity analysis and uncertainty quantification code, RAVEN was used to perform calibration studies for the steady-state portion of PG-27. We developed four PG-27 calibrations based on steady-state conditions. These calibrations all used an effective thermal conductivity equal to 36% of the measured thermal conductivity, but they differed with respect to the frictional pressure drops and radial conduction models. These models all captured the trends in steady-state temperature distributions and transient temperature behavior well. All four calibrations show room for improvement in predicting the transient temperature rise. The smallest error in temperature rise during the transient was a 21% underprediction, and the largest was a 48% underprediction. The errors in transient temperature rise are largely a result of a mismatch in power density between the RELAP5-3D model and the experiment due to the location of active heater rods along the boundary between heat structures in the model. The best of these calibrations was applied to PG-29 to model the DCC. Once again, temperatures during the transient were underpredicted but trends in temperature were captured. The RELAP5-3D model captured trends in the data but could not reproduce measured temperatures exactly. This result is not attributed to deficiencies in the experimental data or to RELAP5‑3D itself. Rather, this result likely arises due to the some of the assumptions and decisions made when the RELAP5-3D model was first developed, prior to the execution of HTTF experiments. An agreement in prediction of temperature trends but challenges reproducing HTTF temperatures within measurement uncertainty is consistent with previous analyses of HTTF in the literature. Future RELAP5-3D validation activities centered around HTTF may be able to provide greater insight into the code's capabilities for HTGR modeling with a more finely nodalized model.

Introduction

The High-Temperature Test Facility (HTTF) is an integral effects thermal hydraulics (T/H) test facility at Oregon State University (OSU) that was constructed to provide validation data for high-temperature gas-cooled reactor (HTGR) T/H modeling. Prismatic block HTGRs are being considered for application as microreactors (Duchnowski et al., 2022; Martin et al., 2022).

Prismatic HTGRs have been deployed previously, including such examples as Fort St. Vrain in Colorado and the High-Temperature Engineering Test Reactor (HTTR) in Japan. The Advanced Demonstration and Test Reactor Options Study identified HTGRs as having a relatively high technology readiness level that could support near-term deployment (Petti et al., 2017). Benchmarks with experimental data for neutronics modeling of prismatic HTGRs exist, including the Very High-Temperature Reactor Critical Assembly (Bostelmann et al., 2016; Bostelmann and Strydom, 2017; Fujimoto et al., 2004) and HTTR benchmark (Bess et al., 2010; Bostelmann et al., 2020). Transient experiments at HTTR can be used to assess multiphysics modeling capabilities for prismatic HTGRs as well (Takamatsu et al., 2014a, 2014b). For integral effects standalone T/H validation of prismatic HTGRs, the Organization for Economic Co-operation and Development–Nuclear Energy Agency (OECD-NEA) HTGR T/H Benchmark, which is based on HTTF data, is being developed (Epiney et al., 2022). This benchmark provides an opportunity for code-to-code and code-to-data comparisons for HTGR T/H models. The experimental data from HTTF provide an opportunity for this benchmark to be used in code validation studies.

This paper presents calibration studies using RELAP5-3D (the Reactor Excursion and Leak Analysis Program, Version 5, three-dimensional code) (The RELAP5-3D Code Development Team, 2018), as well as the Risk Analysis Virtual ENvironment (RAVEN) (Rabiti et al., 2015) sensitivity analysis and uncertainty quantification code. These studies are aimed at validating RELAP5-3D against data from two HTTF experiments: PG-27 and PG-29. The former experiment represents a pressurized conduction cooldown (PCC), and the latter represents a depressurized conduction cooldown (DCC). The PCC occurs when forced circulation of coolant stops due to pump failure, loss of power, or some other phenomenon. During the PCC, the coolant pressure boundary remains intact. Previous work from Idaho National Laboratory (INL) has attempted to model PG-27 but found code predictions to have minimal agreement with the experimental data (Gairola and Epiney, 2021). This paper will demonstrate improved predictions from RELAP5-3D for PG-27. Previous DCC validation efforts from HTTF have focused on the PG-26 experiment (A. Epiney, 2020; Epiney et al., 2021; Kile et al., 2023), but based on confounding factors in the experiment (A. Epiney, 2020), PG-29 has been considered a suitable experiment for DCC validation (Kile et al., 2023). This paper builds on the foundation of HTTF modeling with RELAP5-3D to attempt to validate the code. In general, we find that major trends in the HTTF data are reproduced by the RELAP5-3D models used in this analysis, but transient temperature rises are significantly underpredicted compared to the experimental data. The underperformance of the RELAP5-3D models is attributed to assumptions made when the models were developed rather than based on shortcomings in the RELAP5-3D code itself. This paper provides insight into ongoing code validation activities for a highly relevant reactor concept approaching deployment. We also provide some lessons learned from the existing RELAP5-3D model of HTTF, which can help benchmark participants avoid pitfalls in their modeling activities. This is also the first paper to present best-estimate modeling of PG-29.

Background

HTTF Introduction

HTTF was constructed to perform integral effects T/H testing for prismatic HTGRs. The facility was designed to produce up to 2.2 megawatts (MW) of thermal power through resistive heating. HTTF is a ¼-length-scale representation of the General Atomics Modular High-Temperature Gas-Cooled Reactor (MHTGR), though HTTF is rated for a pressure of 0.7 MPa as opposed to the 6.39 MPa for the MHTGR (Gutowska and Woods, 2019a; Ortensi et al., 2017). HTTF was primarily created for experiments representing a DCC following the blowdown phase of the transient, but it has been used for a low-pressure PCC, as well as lower plenum mixing experiments. The coolant channels in HTTF are full-sized in diameter compared to the MHTGR, and the coolant temperature rise across the core is identical between HTTF and MHTGR (Gutowska and Woods, 2019a). The MHTGR is fueled with Fort St. Vrain-style graphite blocks, whereas HTTF uses an Al_2O_3-based ceramic block. At each axial position, the HTTF blocks contain the inner reflector, the heated rings of the core, and the outer reflector. These blocks are numbered from the bottom up. Block 1 is the block immediately above the lower reflector, and Block 10 is the block just below the upper reflector. The core is heated through 210 resistive heater rods made of graphite. The rods are grouped into 10 banks, with each bank being further divided into three legs (Gutowska and Woods, 2019a). HTTF includes a secondary loop containing a steam generator that is used as the heat sink while the blower is operating. When forced flow stops, heat is removed through the reactor cavity cooling system (RCCS). The RCCS in HTTF is a set of rectangular stainless-steel panels separated from one another by a water flow channel. The innermost RCCS panel is separated from the core vessel by a small air cavity that was not airtight. The RCCS in HTTF uses forced flow to provide heat removal. It is not designed to be representative of the RCCS in the MHTGR, just to provide a radiation heat transfer boundary condition for heat removal in a PCC and DCC (Gutowska and Woods, 2019a).

HTTF Instrumentation

HTTF contains over 500 instruments that were capable of providing high-quality time-dependent data for block and helium temperatures, pressure throughout the facility, gas concentration readings, and data on the secondary loop and RCCS. Though there are large amounts of high-quality data from the HTTF, there is no instrumentation to measure the primary coolant flow rate, though water flow in the secondary loop and RCCS are measured. The core in HTTF is divided into six azimuthal sectors, three of which are instrumented. These are referred to as the primary, secondary, and tertiary sectors, respectively. The primary sector is the most heavily instrumented. The most heavily instrumented locations in the each sector are the tops of Blocks 3, 5, and 7. The radial position of thermocouples (TCs) measuring block temperatures in the primary sector at these axial locations can be seen in Figure 1. Helium TCs are located in positions 6, 8, and 10 (Gutowska and Woods, 2019b). Neither the secondary nor tertiary sectors have a TC at Location 1. The helium and block temperature TCs, aside from the TCs at radial position 18, are R-type TCs. The uncertainty for these TCs is given by the relationship below (Gutowska and Woods, 2019b):

The TCs at position 18 are K-type TCs whose uncertainty is given by the relationship below (Gutowska and Woods, 2019b):

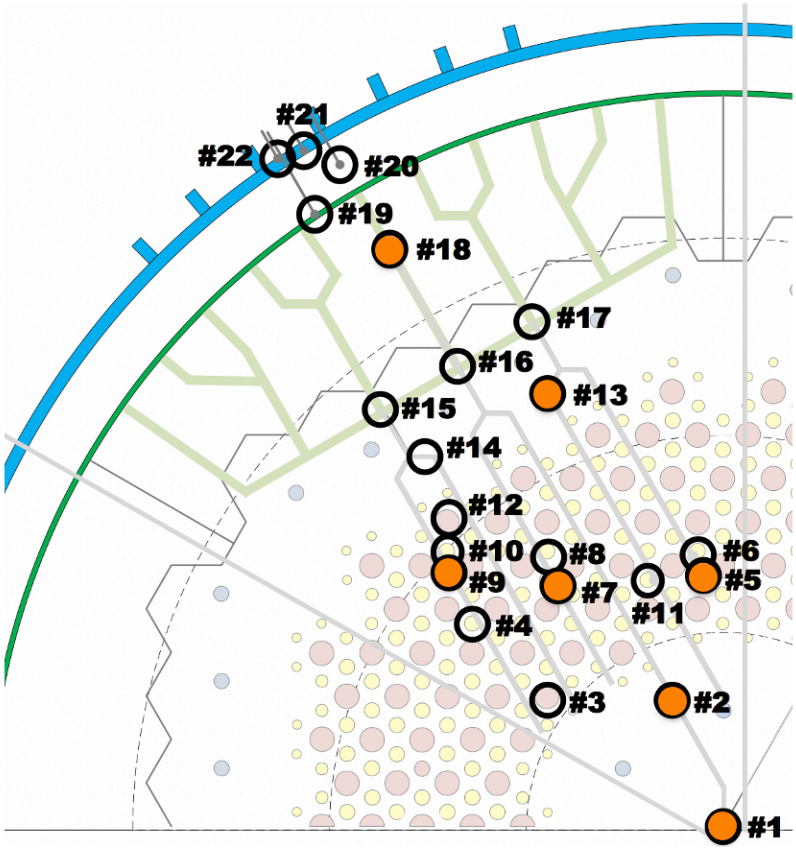

Figure 1: Block temperature TC locations. Adapted from the HTTF instrumentation plan (Gutowska and Woods, 2019b).

For further information about the instrumentation in HTTF, readers are directed to the HTTF instrumentation plan (Gutowska and Woods, 2019b).

HTTF Model in RELAP5-3D

The work presented here uses a RELAP5-3D model that descends from the one developed by Bayless (Bayless, 2018), which was modified by Epiney to bypass the steam generator and provide boundary conditions based on measured conditions at the steam generator inlet and outlet (A. Epiney, 2020). The RELAP5-3D model represents the core as a set of concentric rings. The inner reflector is represented by a set of three rings, with the middle ring containing the inner reflector coolant channels. The core blocks in the heated region of the core are modeled as a set of three rings containing coolant channels. The heater rods are represented as distinct heat structures that are separated from the core blocks by a helium gap. The heater rods communicate with the core blocks only through radiation heat transfer in the model. The

heater rods are not connected to the helium gap. The core blocks are connected to the coolant flow channels on the inside and to the gap between the block and the heater rod on the outside (Bayless, 2018). The outer reflector is modeled as a set of three rings, again with the middle ring containing the coolant channels. The outer reflector is separated from the permanent side reflector (PSR) by a small helium gap. The outer reflector and PSR communicate through radiation heat transfer. The PSR is modeled as a single heat structure. For more details on the RELAP5-3D model, readers are directed to the report describing the model (Bayless, 2018). The model contains enclosures for radial conduction in the inner reflector, heated core, and outer reflector. The middle enclosure contains connections between the inner reflector and heated core and between the heated core and outer reflector (Bayless, 2018).

Measured HTTF data are read into the RELAP5-3D model using an approach documented in a previous RELAP5-3D HTTF modeling report (A. S. Epiney, 2020). The measured data are smoothed with a moving average, then 50 data points are randomly sampled from the smoothed data and put into the model. Then, the 50 points in the smoothed data with the largest derivatives are put into the model to capture points where the state of the facility changed, such as heaters turning on or off, the pump turning off, etc. (A. Epiney, 2020).

The HTTF consists of 10 banks of heater rods, but in the RELAP5-3D ring model, the heater rods in each ring are represented as a single heat structure. In effect, this means that modeling heat being generated in a single heater bank is not possible. Rather, the geometry of the facility is mapped into the model so that if a bank is split 90% in one ring and 10% in another, then 90% of the heat is generated throughout the first of those rings, while 10% is generated throughout the other ring. This, in effect, smears the heat generation out over a larger area in the model than in the facility. The model does not attempt to capture the behavior of the azimuthal sectors separately. Instead, it assumes azimuthal symmetry.

The HTGR T/H Benchmark

The MHTGR-350 benchmark provided neutronics, T/H, and multiphysics code-to-code comparison opportunities (Ortensi et al., 2017). This benchmark highlighted differences in solutions from different toolsets, but it offered no opportunity for validation. In the interest of providing an opportunity for validation of T/H modeling capabilities for prismatic HTGRs, INL, OSU, Argonne National Laboratory (ANL), Canadian Nuclear Laboratories (CNL), the University of Tennessee Knoxville, and other institutions have been collaborating to develop a T/H benchmark based on HTTF data. This benchmark provides an opportunity for both code-to-code comparison and code-to-data comparison for HTTF modeling (Epiney et al., 2022). This benchmark is divided into three problems, each of which is intended to capture different physical phenomena. Problem 1 is aimed at capturing lower plenum mixing and is primarily focused on computational fluid dynamics (CFD) models. As lower plenum mixing is a highly multidimensional phenomenon, it cannot be captured well with one-dimensional (1D) systems codes like RELAP5-3D, so this problem is not modeled in this work. Problem 1 is based on HTTF experiment PG-28. Problem 2 represents a DCC. This problem is primarily intended for systems code modeling. Problem 2 is based on HTTF experiment PG-29. Problem 3 represents a PCC and is also intended primarily for systems code modeling. This problem is based on HTTF

experiment PG-27. All three problems also have the option of coupled systems code/CFD modeling.

Each benchmark problem is divided into multiple exercises. Exercise 1 is a code-to-code comparison exercise. The benchmark will define specific initial and boundary conditions, and benchmark participants will use their codes to solve the problem according to those conditions and compare their answers. Exercise 2 is a best-estimate modeling exercise. Benchmark participants will have access to experimental data from HTTF and can develop their own models to best represent those conditions. Exercise 2 is the code validation exercise. Exercise 3 is an error-scaling exercise that aims to map the relationship between error and uncertainty in HTTF and error and uncertainty in MHTGR-350. Exercise 3 is only intended for Problems 2 and 3. This exercise will provide reference results from the DCC in Problem 2 and the PCC in Problem 3 in the MHTGR-350 based on the ring model (Strydom et al., 2016). A summary of the benchmark problems and exercises can be seen in Table 1.

Table 1: Summary of benchmark problems, exercises, and toolsets. Note: SYS means systems codes and CPL means coupled systems code/CFD models.

Problem	HTTF Experiment	Physics Captured	Exercise 1 Tools	Exercise 2 Tools	Exercise 3 Tools
1	PG-28	Lower plenum mixing	CFD/CPL	CFD/CPL	-
2	PG-29	DCC	SYS/CPL	SYS/CPL	SYS
3	PG-27	PCC	SYS/CPL	SYS/CPL	SYS

Previous HTTF Validation Studies

Previous attempts to validate systems codes and CFD models against HTTF data have met with significant challenges. Prior to discussing those attempts, we introduce the following code assessment descriptors. These descriptors were developed by the U.S. Nuclear Regulatory Commission (NRC) and other institutions in the early 1990s to provide a way to categorize the performance of a code against experimental data (Japan Atomic Energy Research Institute et al., 1993; Schultz, 1993). These descriptors were used by Epiney in previous PG-26 modeling efforts (A. Epiney, 2020) and will be used here to assess the performance of previous modeling efforts, as well as our own modeling efforts:

- **Excellent Agreement:** The code shows no deficiencies in predicting results. Code results are within the uncertainty of the measured data. Using this code for this application will yield correct results.
- **Reasonable Agreement:** The code shows a few minor deficiencies in predicting results, but the major trends in the data are all captured. Code predictions may lie outside the uncertainty bands of the measured data, but they are close to the uncertainty bands. Using this code for this application will yield accurate conclusions, though specific values may not be correct.

- **Minimal Agreement:** The code exhibits significant deficiencies in predicting results. Code results lie well outside the uncertainty in the measured data. Code predictions may be acceptable under some limited circumstances. Some major trends will be predicted correctly, but others are not predicted correctly. Using the code for this application may lead to incorrect conclusions in the future.
- **Insufficient Agreement:** The code has significant deficiencies and cannot provide an acceptable prediction of the results. Major trends are not well-predicted, and code predictions are almost always well outside the uncertainty of the measured data. Use of the code for similar applications is likely to lead to incorrect conclusions.

These code assessment descriptors are still somewhat qualitative. What constitutes a major trend is not clearly defined. Nor is there a clear distinction between data points that are outside but close to the uncertainty bands and data points that are well outside the uncertainty of the measured data. In some circumstances, a case could be made for different descriptors to apply. Nevertheless, these descriptors provide an opportunity to assess code performance with some consistent set of definitions within this work.

In 2020, Epiney used RELAP5-3D to model a DCC experiment from HTTF called PG-26. That work showed significant challenges predicting measured temperatures. Experimental data from PG-26 include a rapid temperature rise for approximately 30 hours, followed by 10 hours of cooldown, followed by a gradual temperature rise until the onset of the DCC. Epiney's work showed a gradual heatup from the initial time until the onset of the DCC. The temperature at 30 hours was significantly underpredicted, and the cooldown from 30–40 hours was missed (A. Epiney, 2020). This work generally showed agreement ranging from insufficient to minimal depending on the figure of merit being assessed or the time period over which it was assessed (A. Epiney, 2020). In a previous paper, we attempted to improve predictions of PG-26 using calibration studies with RELAP5-3D and RAVEN. We generally saw similar underpredictions of temperatures leading to minimal agreement (Kile et al., 2023). ANL has also attempted to model PG-26 using their Systems Analysis Module (SAM) code. That work also showed significant underpredictions of temperatures relative to experimental data (Epiney et al., 2021). In the case of PG-26, the challenges with predicting temperatures are largely attributed to significant uncertainties in the state of the facility. The PG-26 experiment did not include a significant steady-state prior to the onset of the DCC, so developing models that could represent the conditions immediately prior to the onset of the DCC was difficult (A. Epiney, 2020). Lack of measured flow rate data present a significant challenge for modeling PG-26 as well. Additionally, there was a leak of primary coolant during the facility heatup during PG-26. The leak was resolved by overpressurizing the system through the injection of cold helium at 200 K (Cadell and Woods, 2019a; A. Epiney, 2020). No information is provided about the amount of cold helium injected or the rate of injection, making it difficult to model this injection. Absent measured flow data in the core, assessing the impact of the leak on core flow rate and patterns is also difficult. Based on these significant challenges in modeling PG-26, the decision was made to proceed with PG-29 as the benchmark experiment (Kile et al., 2023).

Both ANL and INL have also modeled PG-27 previously using SAM and RELAP5-3D, respectively. PG-27 includes a long period of steady power and steady temperatures prior to the onset of the PCC, which allows the coolant flow rate to be estimated during this steady-state. INL predicted a mass flow rate of approximately 285 g/s prior to the onset of the PCC based on the helium pressure drop through the loop and the pump performance curve (Gairola and Epiney, 2021). ANL predicted a flow rate of approximately 90 g/s prior to the onset of the PCC based on the helium temperature increase through the core (Ooi et al., 2022). The SAM ring model developed by ANL used a calibrated effective thermal conductivity (ETC) equal to 34% of the measured thermal conductivity of the core blocks in an attempt to match block temperatures (Ooi et al., 2022). The previous INL modeling study used the measured block thermal conductivity and conducted sensitivity studies exploring the impact of varying mass flow rate. The helium flow rate was sampled over a range from 30–100% the estimated nominal flow rate. ANL and INL approached PG-27 modeling differently. ANL used the steady-state power, flow, pressure, and inlet temperature conditions to devise a set of steady-state initial conditions for PG-27 modeling (Ooi et al., 2022). INL modeled the entire experiment starting from the initial conditions prior to the onset of heating (Gairola and Epiney, 2021). The INL modeling found that the mean value of steady-state block temperatures at the one location shown in their plots was comparable to the measured temperature from the TC used for comparison, but transient temperatures were underpredicted. The previous INL PG-27 modeling study also included a 90% reduction in block thermal conductivity using the nominal flow rate curve. That analysis showed an underprediction in block temperatures for the entire experiment. Overall, the previous INL PG-27 modeling study can be said to provide minimal agreement with the measured data. Comparison of block temperatures over time in ANL's models showed some locations where temperatures were predicted well, some locations where temperatures were overpredicted, and some locations where temperatures were underpredicted. ANL did not use the code assessment descriptors presented above, but by applying them to their published results, some of the ANL predictions had reasonable agreement with the measured data, while others had minimal agreement. The SAM ring model was able to reproduce PG-27 results better than the RELAP5-3D ring model, though the INL modeling report only compared predicted temperatures to a single TC reading, so detailed assessment of that RELAP5-3D modeling is difficult. Some of the differences between models and the experiment may be due to uncertainties in flow distribution through the core or other uncertainties within the experiment.

The PG-28 experiment was designed to study lower plenum mixing. To help achieve distinct helium exit temperatures in different channels of the core, the heating in PG-28 was azimuthally asymmetric. Both OSU and CNL have modeled PG-28 with RELAP5-3D and STAR-CCM+ (Halsted and Gutowska, 2023; Podila et al., 2022). In both cases, the lower plenum was modeled with a coupled RELAP5-3D/STAR-CCM+ model. RELAP5-3D was used to generate inlet and outlet boundary conditions for the lower plenum, but conditions within the lower plenum were solved with CFD models (Halsted and Gutowska, 2023; Podila et al., 2022). OSU modeling of PG-28 used the RELAP5-3D model developed by Bayless. This model is incapable of capturing the azimuthal asymmetry in the heat distribution. Both the OSU models and the experiment show thermal stratification in the lower plenum, but the models predicted less thermal

stratification than was observed in the experiment. The differences between predictions and experimental data are largely attributed to the RELAP5-3D ring model not providing sufficiently detailed boundary conditions. The OSU team suggested it would be better to use models that can resolve channel-wise temperatures feeding into the lower plenum. The OSU team assessed their models to provide 'reasonable results' (Halsted and Gutowska, 2023). Halsted and Gutowska did not specifically use 'reasonable results' to mean 'reasonable agreement' according to the code assessment descriptors defined by the NRC (Japan Atomic Energy Research Institute et al., 1993; Schultz, 1993), but the agreement between the OSU data and the measured data could likely be called reasonable agreement. The CNL modeling of PG-28 was also aimed primarily at demonstrating a coupling between RELAP5-3D and STAR-CCM+. The CNL model included heat structures representing each of the 1/6 azimuthal segments, so it could capture the asymmetry of the heating in PG-28. The CNL modeling efforts compared standalone RELAP5-3D temperatures, coupled RELAP5-3D/STAR-CCM+ temperatures, and experimental block and helium temperatures in the primary sector of the core at Blocks 3 and 5. At Block 3, CNL models consistently underpredicted temperatures for most of the experiment. At Block 5, the CNL models overpredicted helium temperature and underpredicted block temperature for most of the experiment. Standalone RELAP5-3D models consistently predicted higher temperatures than the coupled RELAP5-3D/STAR-CCM+ models (Podila et al., 2022). Podila et al. defined the agreement between their CNL models and the experimental data 'reasonable' (Podila et al., 2022), but using the code assessment descriptors, it is more accurate to qualify it as minimal agreement. Podila et al. attributes the differences between their models and the experimental data to uncertainties about the flow distribution in the core, as well as the use of region average temperatures instead of individual channel temperatures, which would be a more accurate representation of the TC data.

HTTF was designed to provide prismatic HTGR T/H validation data. BWXT has identified HTTF as a source of integral effects data they intend to use to demonstrate RELAP5-3D capabilities for safety modeling of prismatic HTGRs (Martin et al., 2022). To date, several institutions have compared predictions from multiple modeling and simulation tools—including multiple RELAP5-3D models—to the HTTF experimental data. None have been able to demonstrate excellent agreement between their models and the experimental data. The previous analyses of HTTF experiments PG-27 and PG-28 have generally shown an ability to capture the same trends as are seen in the measured data but reproducing the values from the experiments has been a challenge. The differences between code predictions and the experimental data arise due to a combination of uncertainties in HTTF during the relevant experiments, simplifications, and assumptions made in the relevant models. This work aimed to validate RELAP5-3D against the PG-27 and PG-29 experimental data informed by insights from previous sensitivity analysis on the RELAP5-3D HTTF ring model (Kile et al., 2023).

PG-27 Validation Activities

The first objective in this work was to develop a calibrated RELAP5-3D model based on PG-27. Previous INL modeling of PG-27 with RELAP5-3D attempted to model the entire experiment. The approach in this work was more consistent with the ANL modeling of PG-27. We developed a steady-state calibration to represent conditions in the core prior to the onset of the PCC, and

then used that calibration in the PCC portion of the experiment to assess its performance.

PG-27 Background

PG-27 was an experiment designed to represent a low-power PCC in a prismatic HTGR. The experiment was initially started on 23 April 2019, but due to challenges with water infiltration of the heater rods, the experiment ended up being postponed until 20–24 May 2019. Heater rods were operated for 73 hours, with hours 0–69 representing an initial heatup period. The remainder of the experiment was the PCC itself (Cadell and Woods, 2019b). The power over time from PG-27 can be seen in Figure 2. The power was split between two banks of heater rods, numbered banks 102 and 108. The active heater rods in PG-27 can be seen in Figure 3. These were represented using heater banks 102 and 108 in the RELAP5-3D model developed by Bayless. While the banks in HTTF only cover a 180-degree portion of the core, the nature of the RELAP5-3D model is that each bank is spread around the entire core. In the model, heater bank 102 split its heat generation with 9.5% in the middle heated ring of the core, with the remaining 90.5% in the outer ring of the core. Bank 108 in the RELAP5-3D model split the heat with 14.2% in the middle ring, with the remaining 85.8% in the outer ring. Figure 3 would suggest that the heat distribution between rings in heater banks 102 and 108 should be identical, but we chose to use the heat distribution in the model corresponding to the heater numbers in the experiment rather than attempting to determine an alternate power mapping. There were no banks of heater rods in the RELAP5-3D model that were contained entirely within the outer ring of the core. The heat generation in banks 102 and 108 was nearly identical.

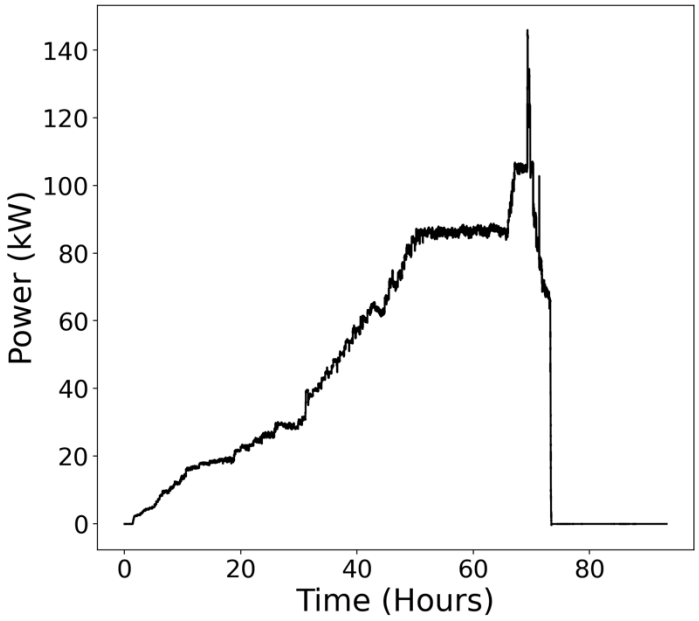

Figure 2: Total power over time in PG-27.

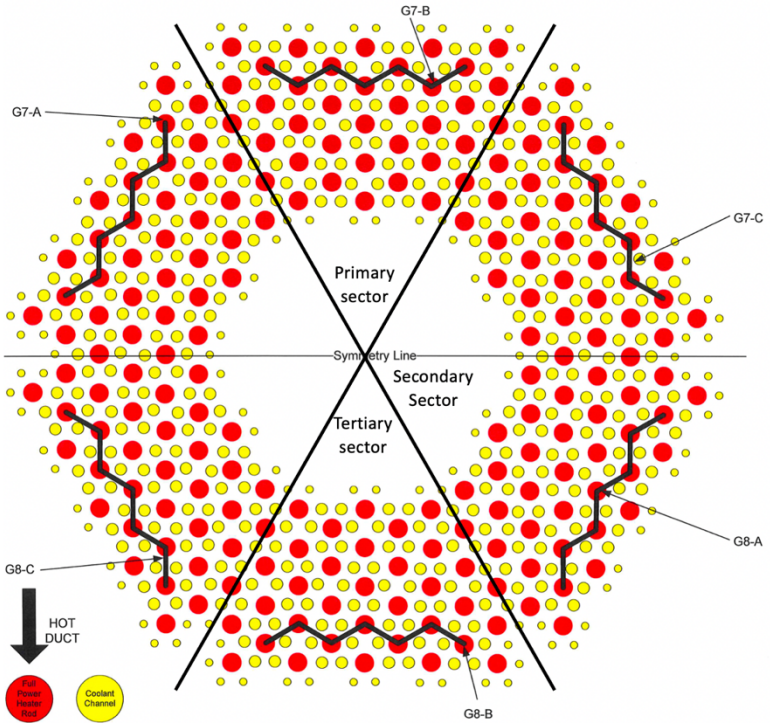

Figure 3: Heater rods used in PG-27.

The period of constant power from hours 50–65 leads to a relatively steady-state condition in the core. Looking at the temperatures over time in Figure 4, this steady state is apparent. That figure represents TCs at TC Location 7 at Block 5. Based on the constant power and temperatures from 50–65 hours, we chose to develop steady-state calibrations based on the conditions at a time of 60-62 hours.

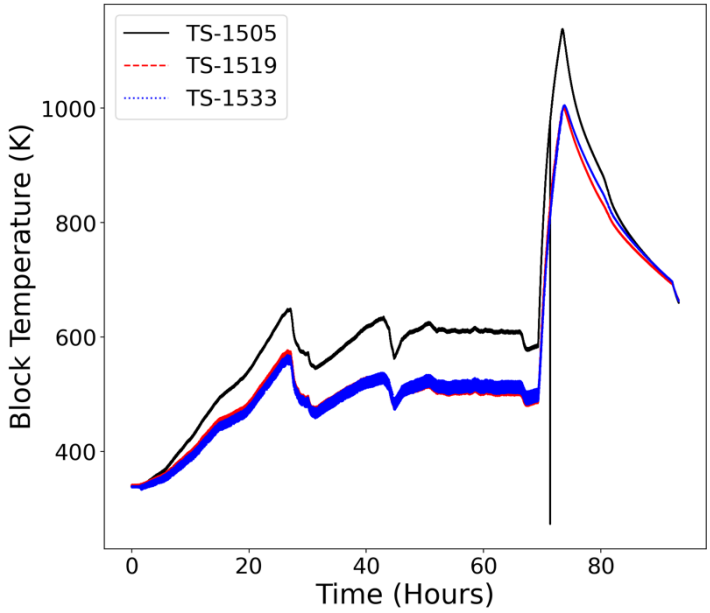

Figure 4: Temperatures over time near the core midplane during PG-27.

Steady-State Calibration

Previous sensitivity studies for steady-state operation at HTTF identified the parameter contributing most to the block temperature prediction was the ETC of the blocks (Kile et al., 2023). Those studies considered a fixed flow rate based on a full-power steady-state. In PG-27, the flow rate was not known, so steady-state calibration studies considered both block ETC and helium flow rate. We introduce the ETC to account for thermal resistance introduced by the holes for the heater rods and coolant channels. The ETC also accounts for possible cracking or other damage introduced in the ceramic block which may reduce conduction through the block.We also considered the impact of increasing friction in each ring to perturb the flow distribution. Our previous HTTF analysis developed an approach for sampling ETC according to unique beta distributions at each temperature (Kile et al., 2023). Block thermal conductivity in HTTF is only measured up to 1,368 K (Gutowska and Woods, 2019a). To provide a thermal conductivity curve up to 2,000 K, Bayless fit the measured thermal conductivity values to a third-order polynomial and extrapolated out to 2,000 K. In this work, the uncertain thermal conductivity space was determined by sampling the curve fit coefficients according to normal distributions to generate 10,000 unique thermal conductivity curves. The standard deviation used in sampling these normal distributions was the uncertainty in the curve fit coefficients from the least-squares regression. The nature of this sampling led to a large number of thermal conductivity values less than or equal to zero. These results were non-physical and based entirely on random sampling of the curve fit coefficients. At each temperature, thermal conductivity values less than or equal to zero were neglected, and the remaining thermal conductivity values were passed into a relationship for ETC developed by Stainsby (Stainsby et al., 2009). Previous T/H studies with 1D codes have used this relationship to account for thermal conductivity degradation due to the presence of coolant channels in the blocks. Those studies found good agreement with the CFD models for conduction heat transfer (Shin et al., 2015).The ETC values were then fit to beta distributions. To verify the beta distributions, we generated a new set of 10,000 thermal conductivity curves, dropped the zero and negative values, and passed them through the same ETC relationship. We plotted the fitted distribution and new values to compare the performance of the beta distribution. Figure 5 shows that at 900 K, the fitted probability density function (PDF) provided good agreement with the new ETC values generated from the curve fit uncertainty calculation. For these steady-state calibration studies, the coolant flow rate was sampled from 5–100 g/s. The lower bound value of 5 g/s was selected based on the lower bound from the previous PG-26 modeling study (A. Epiney, 2020), and the upper bound of 100 g/s based on draft benchmark specifications for Problem 3, Exercise 1. The upper bound of 100 g/s is only slightly higher than the 90 g/s ANL estimates for PG-27 just prior to the onset of the PCC (Ooi et al., 2022). We also sampled friction factors by implementing a friction multiplier in each of the three rings in the RELAP5-3D model. The nominal friction factor in the model can be calculated based on the frictional pressure drop. The frictional pressure drop can then be increased by adding form loss coefficients in the junctions within the pipes that make up the core. This is the same approach that was used by Meehan et al. to implement a magnetohydrodynamic pressure drop in steady-state magnetic fields (Meehan et al., 2022). This approach does not allow users to decrease friction, only to increase friction. Additionally, friction factor is a function of the Reynolds number. This

approach may introduce some error in friction as the flow rate approaches zero. Nevertheless, it provides an opportunity to perturb frictional pressure drop. The friction multiplier was sampled independently in each ring over a range from 1–20. The nominal friction factor was based on a flow rate of 52 g/s, which is the approximate midpoint of the flow rate space sampled in this study. By sampling friction multipliers in each ring independently, we could perturb the flow distribution in the RELAP5-3D model.

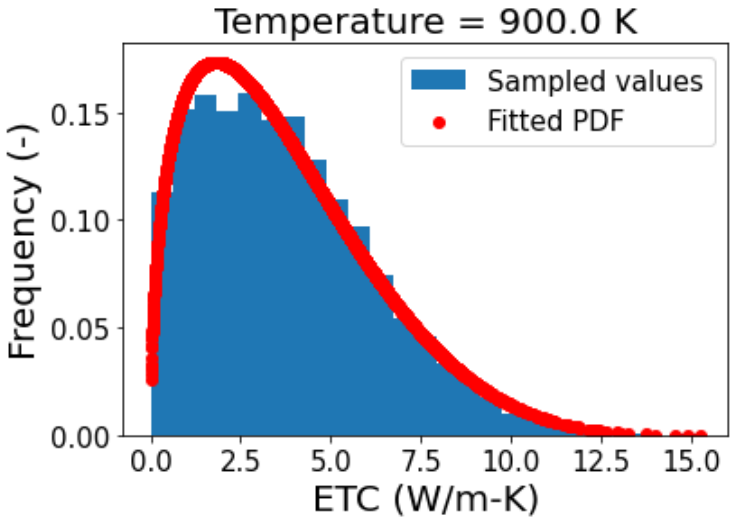

Figure 5: Comparison of fitted PDF and sampled ETCs at 900 K.

The combined ETC, flow rate, and friction calibration study showed that coolant flow rate was by far the most important parameter controlling predictions of block and helium temperatures. To determine the optimum flow rate, we compared the helium temperature increase from vessel inlet to outlet calculated by RELAP5-3D to the measured temperature increase. Figure 6 shows the error in helium temperature increase from these studies. The optimum flow rate was found to be 69 g/s. This is significantly lower than the 285 g/s suggested by previous RELAP5-3D modeling (Gairola and Epiney, 2021), but it is only slightly lower than the 90 g/s suggested by ANL (Ooi et al., 2022). The difference between the 69 g/s value identified here and the 90 g/s value suggested by ANL may be due to the time at which the energy balance calculation was conducted. The value of 69 g/s comes from an energy balance at a time of 62 hours. Figure 4 shows a decrease in block temperatures after approximately 65 hours despite a jump in power from 85 to 105 kW around this time. This decrease in block temperature can be explained by an increase in coolant flow rate after 65 hours.

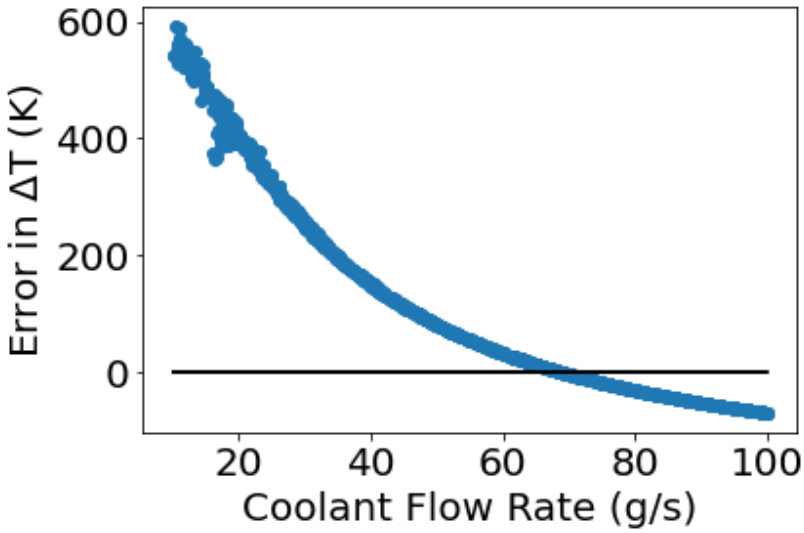

Figure 6: Error in helium temperature rise as a function of coolant flow rate.

Having determined the steady-state coolant flow rate from hours 60–65, we performed an ETC and friction calibration study by perturbing the thermal conductivity of the core ceramic material at each temperature in the thermal conductivity vs. temperature table and applying a friction multiplier in each ring of the model. To determine the most appropriate ETC at each temperature, we compared the ETC to the error in average TC reading at that location. For example, at Block 3, TC Location 5, we compared the RELAP5-3D temperature to the average of the TC reading from the primary, secondary, and tertiary sectors (e.g., all three sectors had functioning TCs at that [r, z] location). A thermal conductivity value was considered accurate if it produced a temperature that was within the 2-sigma uncertainty of the mean temperature. We defined the uncertainty in the mean temperature by propagating the uncertainty from each individual TC reading to the mean temperature. Temperature measurements at a given (r, z) location sometimes vary considerably, like the primary sector TC in Figure 4, which is considerably higher than the secondary or tertiary sectors. This means that the uncertainty in mean TC temperature could be larger using the standard deviation of the TC reading from each sector than using the error propagation approach. The error propagation approach is, nevertheless, appropriate because the mean block temperature is a derived rather than measured value. The TCs are not providing three independent measurements of the same value due to their different azimuthal positions. Additionally, using a smaller uncertainty space allows us to screen out some parameters that may be only slightly important.

We assessed the impact of each parameter by determining the range over which each parameter could bring block temperatures within 2-sigma of the mean temperature at each of the following locations:

- Block 7: TC Locations 5, 7, 9
- Block 5: TC Locations 5, 7, 9
- Block 3: TC Locations 5, 7, 9.

A parameter was deemed unimportant at a given location if one of the following conditions were met:

- No values of that parameter could bring local temperature within the uncertainty of the mean temperature
- Temperatures were within the uncertainty of the local mean temperature across the entire range of that parameter
- There is no clear relationship between the parameter and the local temperature error.

An important parameter is the ETC at 600 K (k_{600}) when compared to the temperature of Block 5 in the middle ring of the RELAP5-3D model. This can be seen in Figure 7, where the temperature error is only within the uncertainty of the mean on an interval from 0.26–5.80 W/m-K. The importance of each parameter was assessed at each of nine locations. If a parameter was defined as important at any of the nine locations, then it was considered important overall. The range over which a parameter was considered globally important was defined as the intersection of the local importance ranges. The parameters that were considered important, as well as their global ranges, can be seen in Table 2.

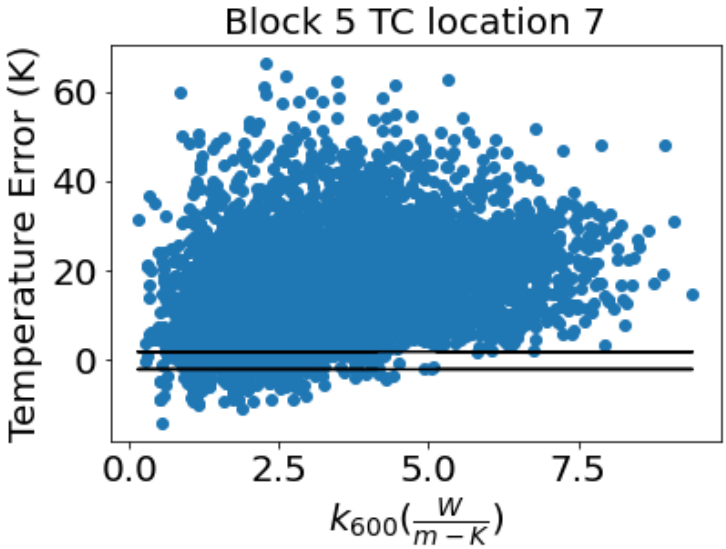

Figure 7: Error in local block temperature at Block 5, TC Location 7, as a function of thermal conductivity at 600 K. Black lines represent the acceptable error bounds

Table 2: Global parameter range for parameters that were considered important in the steady-state calibration study.

Parameter	Lower Bound	Upper Bound	Mean
Thermal conductivity at 500 K (W/m-K)	1.809	1.818	1.8135
Thermal conductivity at 600 K (W/m-K)	1.606	1.825	1.7155
Thermal conductivity at 700 K (W/m-K)	1.038	2.849	1.9435
Thermal conductivity at 800 K	1.963	3.374	2.6685

(W/m-K)			
Outer ring friction multiplier (-)	1.0	11.23	6.115

The range of the outer ring friction multiplier was still quite large even using the intersection of the local parameter ranges. The mean ETC at 500 K is equal to 36% of the thermal conductivity calculated from Bayless's curve fit. As 500 K is within the range of temperatures where thermal conductivity was measured, this comparison is not an extrapolation, and therefore, is appropriate to use here. This is extremely similar to the thermal conductivity multiplier of 0.34 that ANL used in their PG-27 modeling study (Ooi et al., 2022). Based on this, we proceeded to use a scalar multiplier of 0.36 on the thermal conductivity curve fit performed by Bayless to populate the thermal conductivity in this model. Based on the relatively small range of thermal conductivity variation and the large range of friction multiplier in the outer ring, we started by assessing the performance of a standalone ETC calibration.

Figure 8 shows the performance of the ETC calibration at Blocks 3, 5, and 7, as compared to the measured temperatures. Each TC reading includes the 2-sigma uncertainty. Temperatures are defined at a given (r, z) position as 'well-predicted,' if they fall within a space defined by 2-sigma below the lowest measured temperature and 2-sigma above the highest measured temperature. The portion of the core containing heater rods (e.g., TC Locations 5, 7, and 9) is defined by a normalized radius from 0.338 to 0.475. The calibrated RELAP5-3D model always overpredicts temperatures in the inner reflector (normalized radius of 0.0 and 0.18). In the inner ring of the active core, temperatures are well-predicted at Blocks 3 and 5. The temperature of the inner ring is slightly overpredicted at Block 7. RELAP5-3D predicts a temperature of 450 K, but measured values range from 423–425 K. The temperature in the middle ring of the active core is well-predicted at Blocks 5 and 7, but it is significantly underpredicted at Block 3. RELAP5-3D predicts a value of 586 K at that location, but the measured values are 654, 716, and 719 K, respectively. Temperatures in the outer ring (e.g., normalized radius 0.475, TC Location 9), where most of the heat is generated in the RELAP5-3D model, are always underpredicted. The temperature in the outer reflector (e.g., normalized radius of 0.6) is well-predicted at Block 7, but underpredicted at Blocks 3 and 5. Temperatures in the PSR are well-predicted at all axial locations.

The significant underprediction of temperature in the outer ring led to further investigation of friction in the outer ring. The junction loss coefficients used to calculate friction multiplier during the large-scale calibration studies were based on a flow rate of 52 g/s. Those loss coefficients were recalculated for a flow rate of 69 g/s, and the friction in the outer ring was doubled to divert flow from the outer ring in an attempt to bring the outer ring temperatures within the spread of the measured data. Doubling the frictional pressure drop in the outer ring led to a 45% reduction in coolant flow in the outer ring and raised temperatures in the outer ring considerably, as shown in Figure 9. At Blocks 5 and 7, the outer ring temperatures are well-predicted with the increased friction. At Block 3, the outer ring temperature is still too low compared to measured values. The improvement in outer ring temperature at Block 7 comes at the expense of shifting all other temperatures upward to the point that only the outer ring temperature is well-predicted. At Block 5, the new friction in the outer ring causes all

temperatures other than those in the inner reflector and PSR to be well-predicted. At Block 3, the outer ring temperature is still too low, but the outer reflector temperature becomes well-predicted with the increased friction in the outer ring. No location at Block 3 that was well-predicted without the increased friction becomes poorly predicted with the new friction.

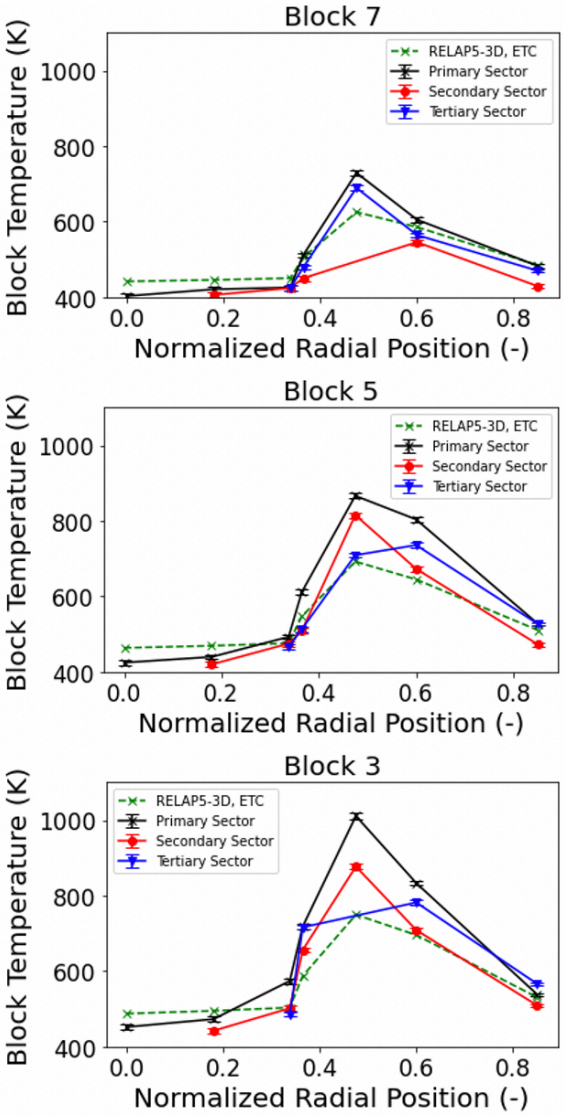

Figure 8: Comparison of RELAP5-3D ETC calibration to measured HTTF temperatures during the steady-state of PG-27.

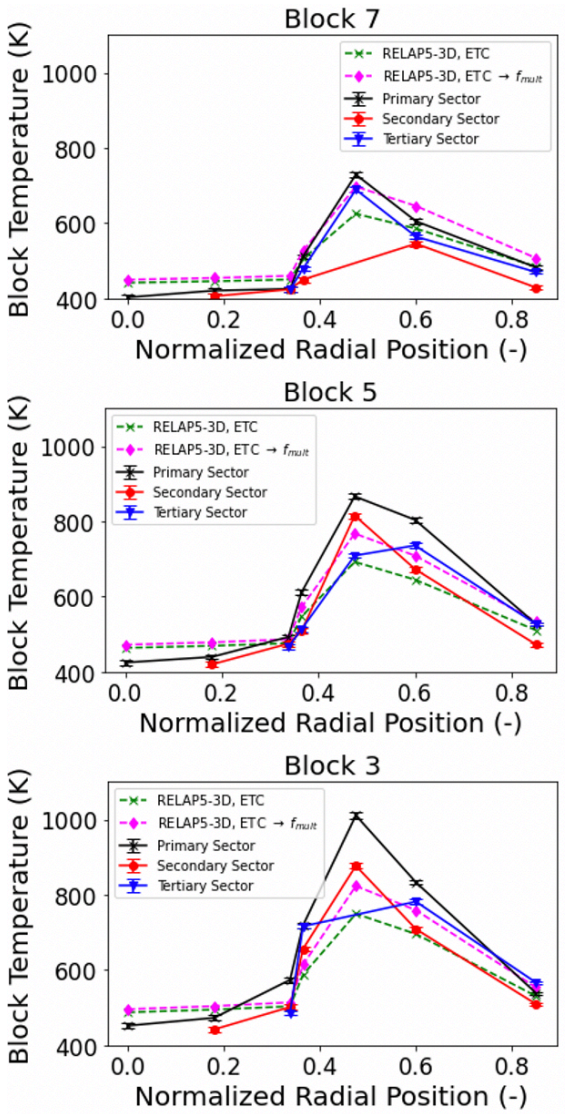

Figure 9: Comparison of standalone ETC calibration and ETC calibration with an additional outer ring friction against the measured data.

To gain further insight into the differences between the standalone ETC calibration and the ETC plus friction calibration, we plotted the helium temperature distributions at Blocks 3, 5, and 7 in the active core, as observed in Figure 10. At Block 7, both calibrations predicted helium temperature well in the inner ring, neither calibration predicted helium temperature well in the middle ring, and only the increased friction calibration predicted the helium temperature well in the outer ring. At Block 5, both calibrations underpredicted temperature in the inner and outer rings, but the high friction calibration predicted a helium temperature within the uncertainty of the secondary sector TC measurement. At Block 3, the high friction calibration predicts temperatures well in the inner and outer rings, but the middle ring temperature is underpredicted. The standalone ETC calibration does not predict any helium temperatures well at Block 3.

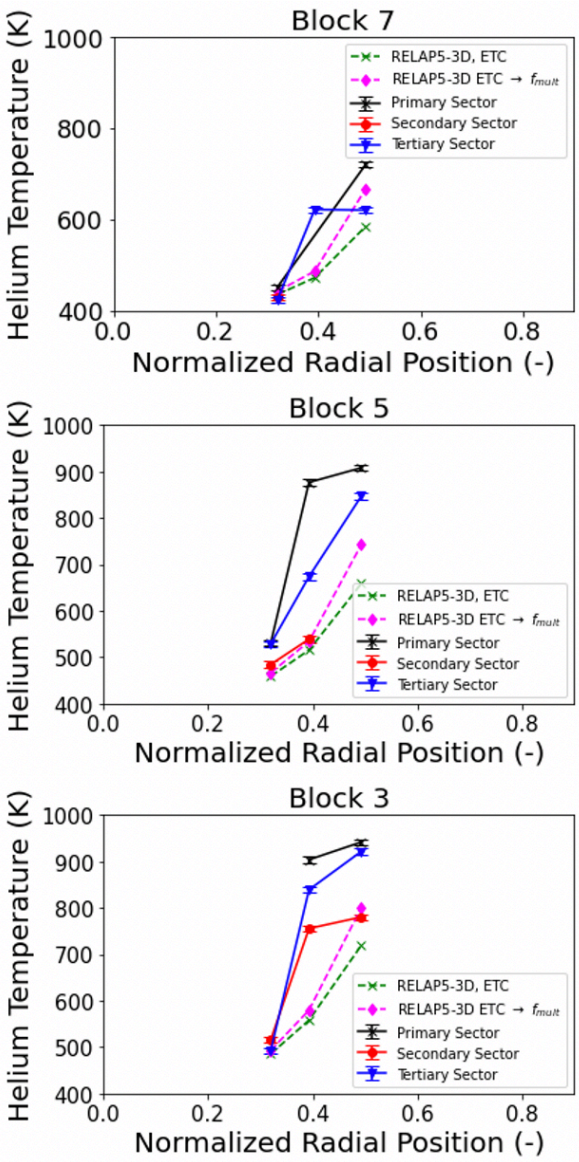

Figure 10: Steady-state helium temperature distributions in the experiment and the two RELAP5-3D models.

The assessment of helium temperature agreement is more challenging than block temperature agreement due to a larger number of failed instruments and a smaller number of TC locations. For example, helium temperatures in the middle ring of Block 7 can only be assessed against a single TC. At Block 5, the helium temperature according to the ETC plus friction calibration is slightly below the secondary sector TC in the inner ring and within the uncertainty of the secondary sector TC in the middle ring, but the helium temperature in the outer ring at Block 5 cannot be compared to the secondary sector TC because there is no secondary sector reading there. Based on steady-state helium temperatures, the ETC plus friction calibration performs better than the standalone ETC calibration. This could be because the higher friction calibration captures the coolant flow distribution better, or it could be because temperatures are underpredicted in the standalone ETC calibration and reducing flow in the outer ring just masks that effect.

There are still some uncertainties in HTTF that have not been captured in these steady-state calibrations. For example, in the middle ring of the core, both block and helium temperatures are well-predicted at Block 5, but at Block 3, block and helium and block temperatures are significantly underpredicted. The dramatic shift from well-predicted at Block 5 to significantly underpredicted at Block 3 could be indicative of a shift in the flow distribution between Blocks 3 and 5. The RELAP5-3D model does not include crossflow or bypass flow between the different rings. It is entirely possible that flow may have been diverted around the TC at Block 3, Positions 7 and 8 (e.g., block and helium TCs, respectively) and led to higher temperatures there. The RELAP5-3D model simply cannot capture this behavior that may have occurred. Figure 8, Figure 9, and Figure 10 all show positions in which the primary, secondary, and tertiary sector TCs measure dramatically different temperatures from one another. Based on heater distribution, the temperatures in the primary, secondary, and tertiary sectors should be similar to one another assuming no complications are present that may introduce some asymmetry. The dramatic difference in temperatures between sectors may indicate some unintended asymmetry in the experiment that the RELAP5-3D model cannot capture. The differences in temperature readings in each sector may be a result of power maldistribution, localized damage in core block material, TC misplacement or shifting, or other effects. Without further information, we cannot identify the cause of the dramatic difference in temperatures across the sectors.

Transient Calibration Testing

To further assess these calibrations, we applied them to models that included the PCC portion of the experiment. These models used the steady-state solutions presented above as their starting point and applied boundary conditions starting at a time of 60 hours. The PCC itself begins at a time of 69.3 hours. Figures assessing these calibrations starting at 60 hours will use the 60-hour mark of the experiment as time zero—meaning the PCC starts at a time of 9.3 hours. Both RELAP5-3D calibrations significantly underpredicted the temperature rise during the transient part of the experiment. Figure 11 shows some results that are typical of the behavior seen throughout the rings containing heater rods. Figure 12 shows the results from TC Location 1, where the temperatures were overpredicted in steady state. Even when the steady-state temperature is overpredicted, the transient temperatures are underpredicted. Table 3 shows the temperature rise in the rings containing heater rods. The measured values reported in Table 3 are the mean of the measured value from each working TC corresponding to the (r, z) location. This temperature rise is defined as the difference between peak temperature and initial temperature. The standalone ETC calibration predicts a higher temperature rise in the outer ring of the core than the ETC plus friction calibration, but this is expected given the higher flow rate in the outer ring from the standalone ETC calibration. Increasing friction in the outer ring leads to a larger temperature rise in the inner ring, but only by about 20 K. This difference is not significant compared to the 140–180 K difference between measured and predicted temperature rise in the standalone ETC calibration, which underpredicts the temperature rise by 28–41%. The ETC plus friction calibration underpredicts the temperature rise by 28–48%.

Previous analysis of HTTF thermophysical property uncertainty showed very low uncertainty in the volumetric heat capacity of the core blocks. That low uncertainty led to a low impact on

peak temperatures from changing heat capacity (Kile et al., 2023). Differences in heat capacity over the relevant temperature range for PG-27 fluctuate from 4–16%; however, even a 16% reduction in heat capacity would be insufficient to eliminate the 28–48% underprediction in block temperature rise.

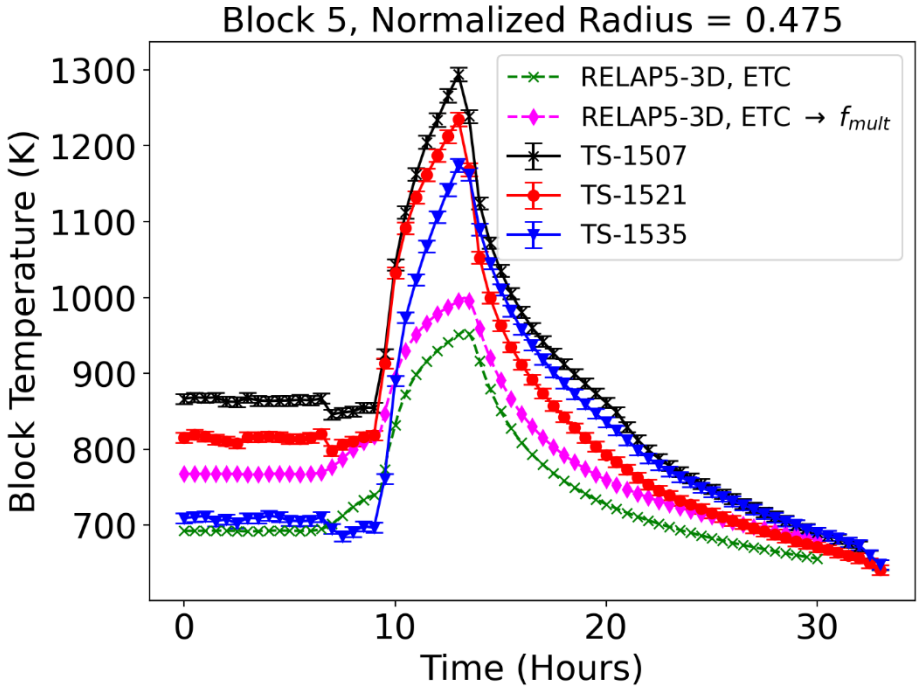

Figure 11: Temperatures at Block 5, TC Location 9. TS-1507 is in the primary sector, TS-1521 is in the secondary sector, and TS-1535 is in the tertiary sector.

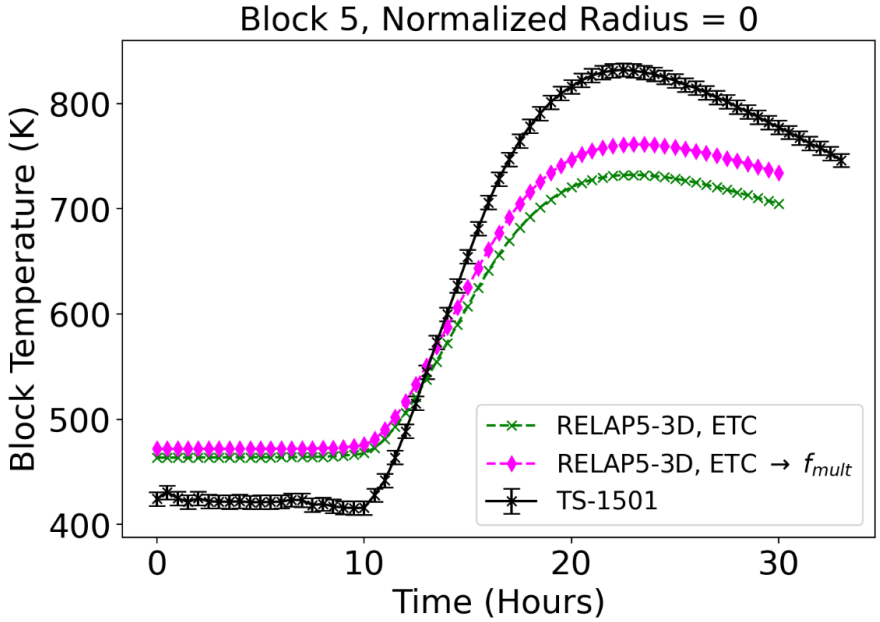

Figure 12: Temperatures at Block 5, TC Location 1.

Table 3: Temperature rise (K) at each location. Values are Measured | ETC calibration | ETC + friction calibration.

	Inner Ring	Middle Ring	Outer Ring

Block 7	480|305|327	552|324|232	505|300|272
Block 5	487|297|317	504|306|317	453|263|232
Block 3	424|284|304	426|286|295	322|232|202

New Radial Conduction Models

In the PCC, radial conduction is a significant heat transfer mechanism. In the original RELAP5-3D ring model, Bayless used three conduction enclosures to capture this radial heat transfer. All three enclosures used the same table for temperature-dependent conductance (Bayless, 2018) despite having different ratios of block, helium, and heater rod graphite. Bayless accounted for these differences by modifying the conduction area factors in the RELAP5-3D model to account for the ratio of local conductance to the conductance used in the temperature-dependent conductance table. That ratio was determined at 900 K using the measured block thermal conductivity. In the analysis presented thus far, we varied the temperature-dependent conductance table based on our changes in block thermal conductivity, but we did not change the conductance ratios in the area factors. The approach that Bayless used when setting up these conduction enclosures to use a single temperature-dependent conductance table with conductance ratios built into the area factors is an approximation that may be useful and could introduce a small error at temperatures typical of a full-power steady-state. It is more likely to introduce meaningful error when temperatures are frequently below 900 K, as is the case in PG-27. To explore the impact of this assumption, we developed new temperature-dependent conductance data for each of the three conduction enclosures The new radial conduction models lead to a conductance in the rings containing heater rods that is 5–10% higher in the heated rings than the Bayless approach using the ETC. The conductance in the inner reflector is lower than the conductance calculated using the Bayless approach with the ETC. Below 500 K, the conductance of the outer reflector is higher than the Bayless ETC conductance; but above 500 K, the conductance of the outer reflector is lower than the Bayless ETC conductance. This can be seen in Figure 13.

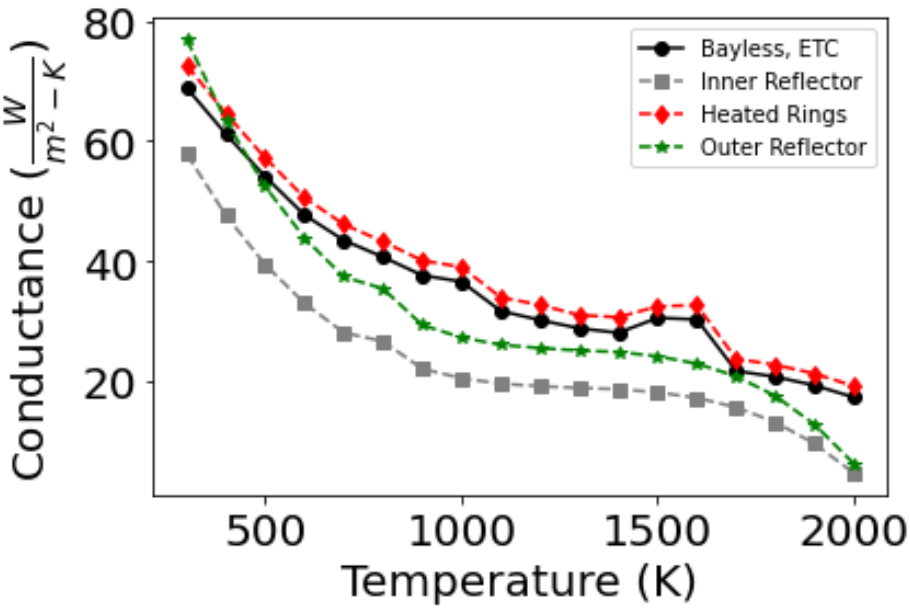

Figure 13: Comparison of different conductance data.

The new radial conduction model was applied to the standalone ETC calibration and ETC plus friction calibration discussed above. As shown in Figure 14, the new conductance model led to slightly lower temperatures in the inner reflector. The conductance in the region containing heater rods (the core region) is only slightly higher with the new conduction model, and temperatures in that region are comparable between the old and new conduction models. The new temperatures are slightly lower due to the slightly greater conduction heat removal, but this difference is on the order of 10 K or less in the core region. Temperatures in the outer reflector are lower with the new radial conduction models.

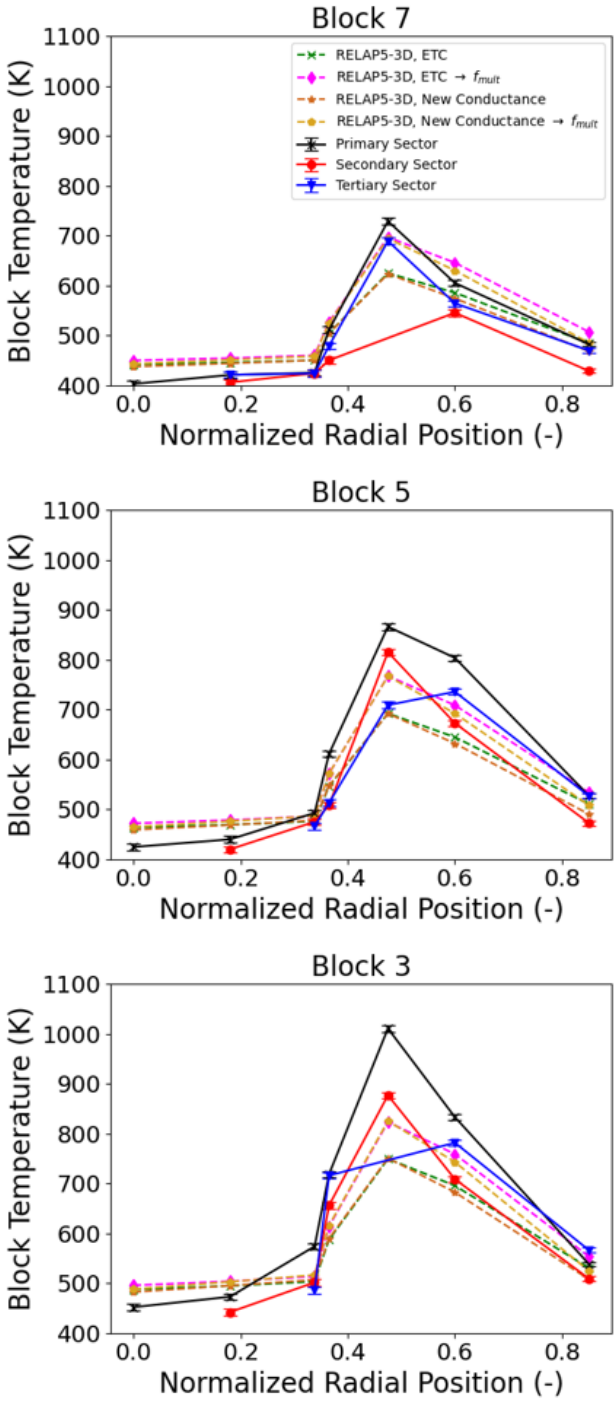

Figure 14: Steady-state temperatures from the RELAP5-3D calibrations with and without the new conductance model.

Steady-state temperatures were lower with the new radial conduction models than the old ones. As a result, a few temperatures that were overpredicted using the old conduction model are now well-predicted, but this improvement is confined to the permanent reflector. The temperature in the permanent reflector at blocks 5 and 7 went from over-predicted when the old conduction model was used with the ETC plus friction calibration to well-predicted when the new conduction model was used in conjunction with the ETC plus friction calibration. There

was no instance in which a location was well-predicted using the old conduction model and not well-predicted using the new conduction model. During the PCC portion of the experiment, the temperature rise was improved using the new radial conduction models. In the outer ring of the core, where approximately 90% of the heat is generated, the temperature rise is higher using the new conduction model. In the other rings of the model, the temperature rise in the core is comparable between the new and old conduction models. Figure 15 shows that even though the steady-state temperatures for the calibrations with the new conduction models start at significantly lower temperatures than their counterparts with the old radial conduction model, the peak temperatures during the PCC are comparable. Given the lower conductance—and therefore lower radial conduction heat transfer—in the inner and outer reflectors with the new conduction implementation, the larger temperature rise during the PCC is an expected result. However, this larger temperature rise is still well below the measured temperature rise in the experiment. Table 4 shows the temperature rise of the models with the new radial conduction implementation compared to the temperature rise in the experiment. The standalone ETC calibration with the old radial conduction model underpredicted the temperature rise by 28–41%. The same ETC calibration with the new radial conduction model underpredicts the temperature rise by 21-37%. The ETC plus friction calibration with the old radial conduction model underpredicted the temperature rise by 28–48%. The ETC plus friction calibration with the new radial conduction model underpredicts the temperature rise by 22-44%.

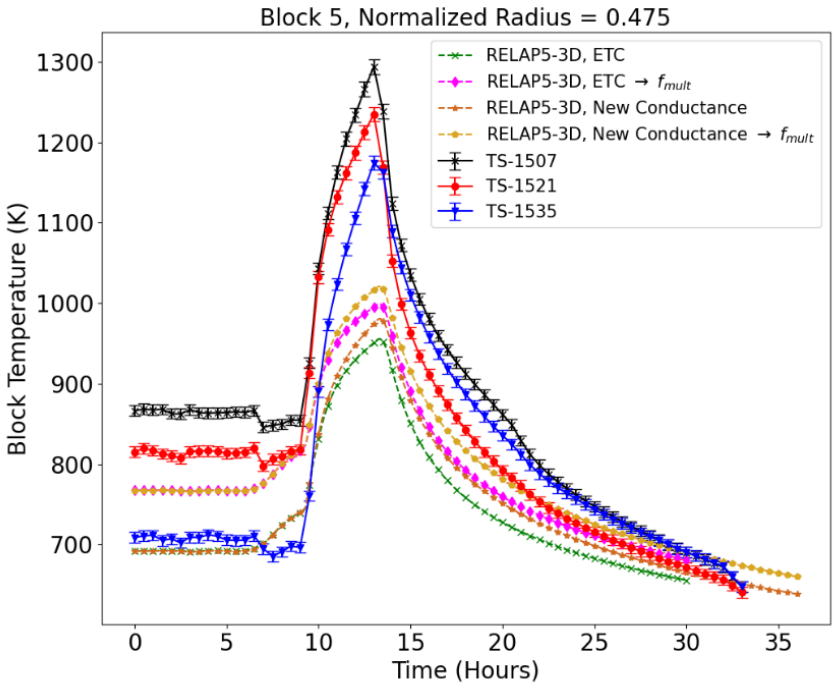

Figure 15: Temperatures at Block 5, TC Location 9 during the PCC.

Table 4: Temperature rise (K) at each location. Values are Measured|ETC calibration|ETC + friction calibration. Both calibrations use the new radial conduction model.

	Inner Ring	Middle Ring	Outer Ring
Block 7	480|336|358	552|349|363	505|327|294
Block 5	487|326|347	504|330|341	453|289|254
Block 3	424|311|331	426|308|317	322|256|222

In summary, the new radial conduction models predict comparable temperatures in the part of the facility generating the most heat during steady-state, and the temperature rise in the same part of the core is higher during the PCC portion of the experiment. We thus conclude that the new conduction models represent an improvement in code predictions in the core region over the old conduction models.

Limitations of the RELAP5-3D Model

All four models of PG-27 that have been presented contain significant differences between their predictions and the experimental data. These models can be said to show only minimal agreement with the HTTF data. Steady-state temperatures are sometimes well-predicted, and the shape of the steady-state temperature distribution is generally captured, though the minimum is too high, and the maximum is sometimes too low. The transient temperatures capture the major trends in the HTTF data. The initial dip in temperature from hours 65–69 is not captured, but this is because we maintained a constant flow rate from hours 60–69, not because RELAP5-3D is incapable of modeling that temperature dip. The most concerning difference between the RELAP5-3D results and the experimental data is the significant underprediction in temperature rise during the PCC. The block thermal conductivity that was used in these models is approximately 36% of the measured block thermal conductivity. The ETC relationship that was developed by Stainsby (Stainsby et al., 2009) and verified by Shin et al. (Shin et al., 2015) would only lead to a 20–25% reduction in thermal conductivity rather than the 64% reduction in thermal conductivity that was required to reproduce steady-state temperatures in PG-27.

The reports defining the code assessment descriptors used in this work recommend revisiting the nodalization of a model when agreement is less than excellent (Japan Atomic Energy Research Institute et al., 1993; Schultz, 1993). Considering the nodalization of the RELAP5-3D ring model and the heat generation profile in PG-27, the nodalization may be a significant driver of the differences between the model and the experiment. Figure 16 shows the regions of the core that generated heat in the experiment and the RELAP5-3D model. In the experiment, the heater rods connected by black lines generated heat. In the RELAP5-3D model, the heat was split between the outer and middle rings. In total, 20% of the heater rods (e.g., 42 out of 210) were used in the experiment. In the RELAP5-3D models, the ring model distributes the same amount of heat through heater rod heat structures with a volume equivalent to 73% of the heater rods because each ring contains only one heat structure representing all the rods in that ring. This leads to a significantly lower peak power density in the RELAP5-3D model than was seen in the experiment. The RELAP5-3D model essentially averages heat generation over a large

region, most of which is unheated in the experiment. This much lower peak power density in the RELAP5-3D model than the experiment requires a significant degradation in thermal conductivity to produce comparable block temperatures between the model and the experiment. This smearing of the power density also leads to considerably lower coolant temperatures in the outer ring of the core. Increasing friction in the outer ring to reduce the flow rate during steady-state masks this effect, but the shortcoming of masking that effect is made clear when comparing the temperature rise in the outer ring between the models with and without the increased friction. Reducing the power density by spreading out the heat generation to a much larger fraction of the core also drives the significant differences in temperature rise during the PCC. The RELAP5-3D model is attempting to reproduce local temperature measurements reported by the TCs but is using significantly different local power densities. A model with a finer radial nodalization may be able to reproduce local temperatures and the transient temperature rise better.

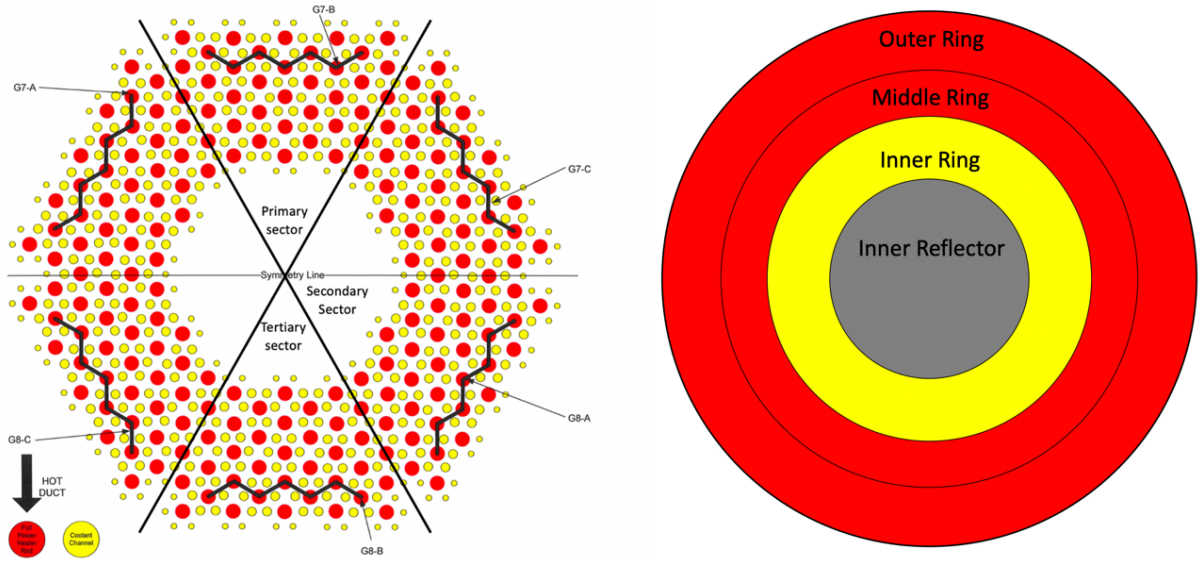

Figure 16: Comparison of heat generating location in the experiment (left) and the RELAP5-3D model.

PG-29 Validation Activities

Having developed a calibrated ETC based on the PG-27 steady-state, we applied that calibration to PG-29, a low-power DCC experiment. Given the shortcomings of the calibration when applied to PG-27, this analysis was not expected to reproduce the temperature rise from PG-29. This study simply sought to ensure that the PG-27 calibration was capturing physics rather than the particulars of the PG-27 data set. If the PG-27 calibration applied to PG-29 demonstrated some anomalous behavior like significantly overpredicting temperatures or temperature rise during the DCC, that would suggest some overfitting in the PG-27 calibration.

PG-29 Background

PG-29 was an experiment performed from 24–26 July 2019, representing a DCC with asymmetric heat generation. In HTTF, the DCC is represented by opening valves connecting the primary coolant loop to a volume known as the reactor cavity storage tank. PG-29 was

performed immediately following PG-28, a lower plenum mixing experiment that used an asymmetric heating profile. The distribution of active heater rods in the core can be seen in Figure 17. The actual PG-29 experiment started at 9:15:32 p.m. on 24 July 2019. The models used in this analysis start from the conditions at 3:42:20 p.m. on 24 July 2019. This is done because the pump speed—and correspondingly the coolant flow rate—varies from 30–32% of the rated speed during the course of the experiment (Nakhnikian-Weintraub et al., 2019), and starting the models at 3:42:20 p.m. on 24 July 2019 provides a long period of time in which pump speed was constant, thus allowing a steady-state to develop prior to the onset of the DCC. The power over time used in these models can be seen in Figure 18. The DCC itself is initiated at a time of 8 hours. The heaters are turned off at a time of 17 hours. The exact flow rate prior to the onset of the DCC is unknown. Immediately following the end of PG-28, the pump speed in HTTF was ramped down from 60% to 30%. Halstead and Gutowska estimate the primary coolant flow rate at that time to be between 60 and 70 g/s (Halsted and Gutowska, 2023). PG-29 contained 19 block temperature TCs that were non-functional (Nakhnikian-Weintraub et al., 2019). Given the asymmetry in the power distribution, non-functional instruments in one sector of the core make it impossible to determine the temperature in that sector. Despite the challenges imposed by the asymmetry, PG-29 was considered a suitable experiment for this comparison because there were no unanticipated events that occurred during the experiment.

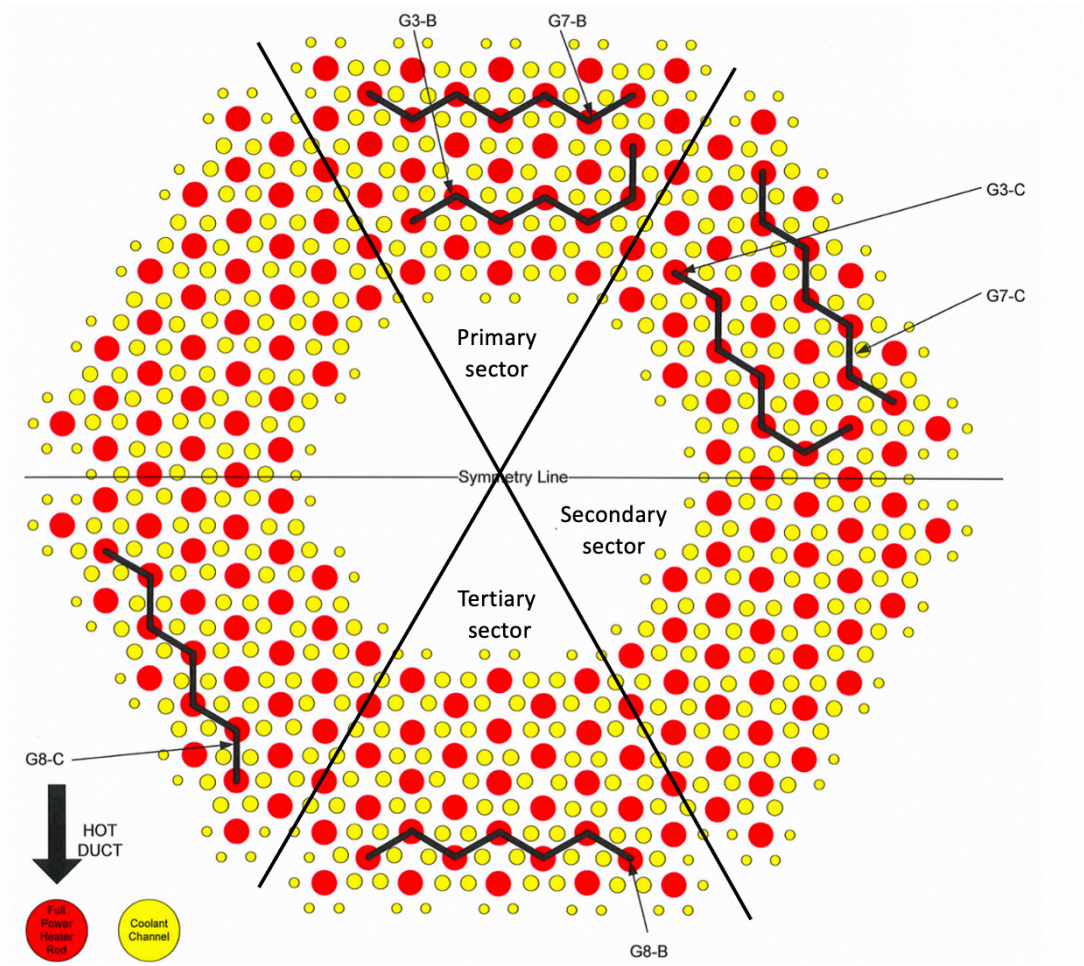

Figure 17: PG-29 active heater rod distribution. Heaters connected by black zig-zag lines are the active rods.

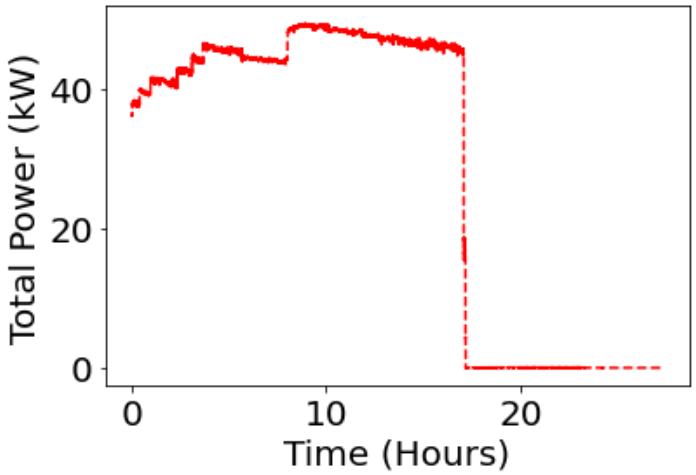

Figure 18: Power over time in the PG-29 models. DCC is initiated at 8 hours and heaters are shut off at 20 hours.

Calibration Testing

Given the asymmetry in PG-29 and the azimuthal symmetry in the RELAP5-3D model, the model cannot be directly compared to the reading from any individual TC during this experiment. The inability of the calibrated ring model to match the temperature rise during the PCC in PG-27

also provides strong reason to suspect that the temperature rise in PG-29 would be underpredicted. Based on the symmetry in the RELAP5-3D model, we know that the peak power density will not be captured in the model. Based on the location of active heater rods in PG-29, all three rings of the RELAP5-3D model were used for PG-29. Based on this figure, we determined the active heater banks were 102, 107, and 108. Banks 102 and 108 are the outer set of heaters in the primary and tertiary sector. Heater 107 corresponds to the rods that were active in the inner set in the primary sector. Absent any information about specific power fraction in each heater bank, we assumed that the heat was split evenly between the three heater rod banks. We chose to put all of the heat from heater 102 into heater 108, which is acceptable given the symmetry in the RELAP5-3D model. Thus, the RELAP5-3D model split the heat such that 2/3 of it was in heater 108, while the other 1/3 was in heater 107. The goal of this analysis was to assess the performance of the RELAP5-3D calibration by looking at two things:

- The shape of the temperature vs. the time curve in RELAP5-3D
- Whether or not the RELAP5-3D results are somewhere within the spread of the measured data.

When the core is heated, the RELAP5-3D model should produce temperatures that are within the highest and lowest measured temperatures. The lowest temperature will come from the unheated secondary sector. The highest temperature will come from either the primary or tertiary sector. With the heat generation smeared throughout all six azimuthal sectors, the RELAP5-3D model should produce temperatures that are somewhere in between those of the heated and unheated sectors of the core. If the RELAP5-3D temperatures were outside the spread of the measured temperatures while the heater rods were running, then the calibration may be inappropriately fitting the PG-27 data instead of capturing the physics of conduction cooldowns in HTTF.

Halstead and Gutowska estimated the flow rate immediately following PG-28 to be between 60 and 70 g/s (Halsted and Gutowska, 2023). The pump speed was varied during the actual PG-29 experiment. Rather than trying to capture the flow rate evolution during the 8 hours prior to the onset of the DCC, we developed two models with a constant flow rate of 60 and 70 g/s prior to the DCC. These models used the standalone ETC calibration with the new radial conduction model. We selected this calibration because it most accurately captures the temperature rise during the PCC with the smallest error in the rings containing heater rods. The temperature at the beginning of the models was defined as the average temperature of the working TCs at that location. If a location did not have any functioning TCs, then the temperature was calculated via linear interpolation based on the temperatures above and below that location. Figure 19 shows the temperatures vs. the time in the inner ring of the RELAP5-3D model. The results show the RELAP5-3D temperatures decreasing from their initial value for approximately 2.5 hours. After that 2.5-hour period, temperatures have reached a relatively steady-state prior to the onset of the DCC. The steady-state temperature sits between the temperature of the tertiary sector TC and the secondary sector TC. The temperature likely lies between these two due to the smearing of power throughout the core rather than in discrete sections. That the RELAP5-3D models predict a temperature within the spread of the measured values in this steady-state is

encouraging. The steady-state temperature for the 60 g/s model is 10 K hotter than the 70 g/s model. During the transient, the temperature rise between the 60 and 70 g/s models differs by just 1 K. After the 2.5-hour equilibration, the temperature in the RELAP5-3D models demonstrate the same trend as the temperatures from the heated portions of the core and the mean TC temperature. Temperatures rise following the onset of the DCC until the heaters are shut off at 17 hours. At that point, the temperatures in the heated portions of the core begin to fall, as does the average TC temperature. The temperature in the secondary (unheated) sector of the core continues to rise after the heaters are shut off. This occurs because in the facility, heat moves both radially and azimuthally through the core. The RELAP5-3D models begin to cool down at 17 hours, and eventually, the temperatures predicted by the models fall below the secondary sector TC reading. This is a result of the azimuthal symmetry in the RELAP5-3D models, because in RELAP5-3D, the heat can only be removed radially, leading to more rapid cooldown of the whole core. The behavior shown in Figure 19 is representative of the behavior in the other locations in the heated rings containing functioning TCs in all three sectors.

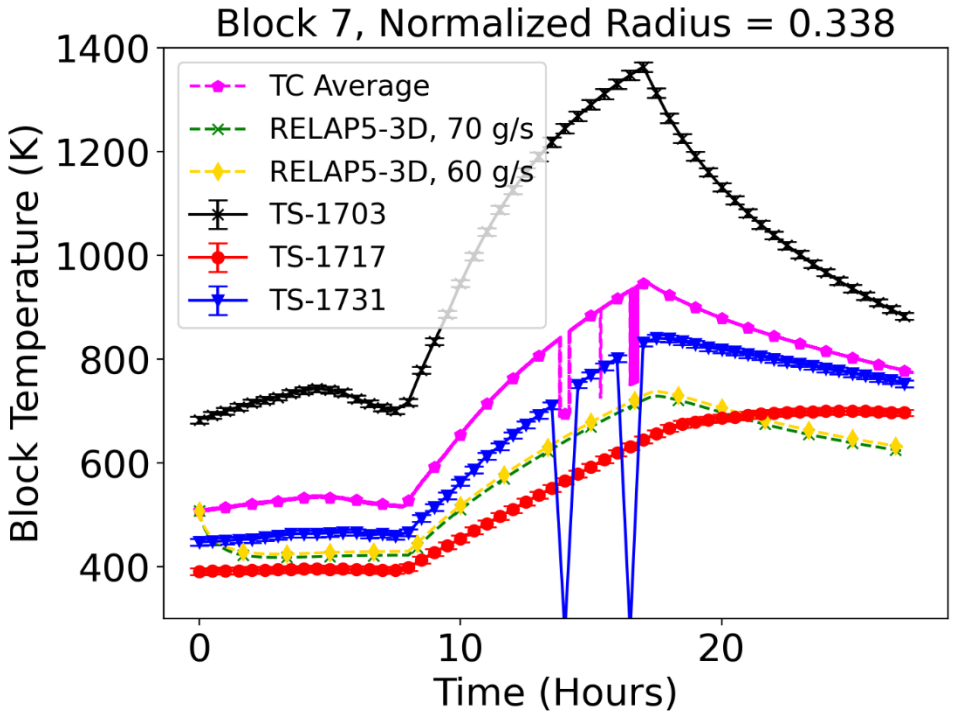

Figure 19: RELAP5-3D and measured block temperatures during PG-29 at Block 7, TC Location 5.

Given the challenges introduced by the asymmetry of PG-29 and the limitations of the RELAP5-3D model, the results from the PG-29 analysis are as good as can be expected. The performance of the PG-27 calibration applied on PG-29 does not show any serious deficiencies that cannot be explained by the asymmetry in the experiment or the coarse radial nodalization of the model. To perform better validation analysis, models capable of capturing the asymmetry of the heating in the experiment should be used.

Conclusions

We have presented calibration studies of the RELAP5-3D ring model of HTTF aimed at validating that model. We performed calibration studies to reproduce steady-state temperatures in PG-27, and then used those calibrations to model the PCC portion of the experiment. The standalone ETC calibration generally underpredicted steady-state temperatures in the outermost ring of the core, but by doubling the frictional pressure drop in the outer ring, steady-state temperatures could be reproduced in that region of the core. Both calibrations underpredicted the transient temperature rise by 28–48%. To improve the transient performance of the calibrations, we developed a new radial conduction model that better captured local variations in conduction heat transfer. The new conduction models led to comparable steady-state temperatures, and a larger temperature rise during the PCC portion of the experiment. The error in temperature rise ranged from 21–44% when the new conduction models were used. Agreement between RELAP5-3D and the experimental data from PG-27 was determined to be minimal. The challenges associated with predicting temperature rise in RELAP5-3D are likely a result of the model rather than deficiencies in the code itself. The model was developed prior the execution of the experiments, and the location of heater rods used in the experiment leads to some distortions in power density in the model when total power is preserved. The model distributes heat throughout 73% of the heater rod volume in PG-27, whereas in the experiment, only 20% of the heater rods were used. The distortion in power density between the model and the experiment was identified as the likely cause of the significant reduction in thermal conductivity compared to expected ETC values based on HTTF block geometry. The lower power density in the RELAP5-3D models, which arises due to the nodalization, is also the likely cause of the underprediction in temperature rise. The standalone ETC calibration with the new radial conduction model was applied to models of PG-29 with two different flow rates to provide an additional check on the calibration. The asymmetry of the heat generation in PG-29 could not be captured in the model. The same challenges with underestimating the power density were identified prior to running the models. The goal of the PG-29 comparison was to determine whether the calibrated model could produce temperatures in between the hottest and coldest PG-29 temperatures. While the heater rods were running, the RELAP5-3D models produced temperatures within the spread of the TC measurements. The models also reproduced trends in the PG-29 data for the heated sectors of the core, even if the specific temperature values could not be matched. This provides confidence that the calibration is not just fitting the specific temperature distributions in PG-27 but capturing the physics of the facility and the experiment as well as is possible given assumptions inherent in the RELAP5-3D model.

These studies, like others before them, have demonstrated only limited validation against the HTTF data. Our inability to fully validate the ring model against the PG-27 and PG-29 data is not primarily attributed to any problems with the data sets or to deficiencies with RELAP5-3D itself. Rather, it is likely a result of the model struggling to capture the local differences in power density in the core correctly. Analysts who wish to assess the capability of RELAP5-3D or other 1D systems codes to model the PCC and DCC transients should ensure their models accurately capture the power distribution and the total power. There may be uncertainties in the HTTF

data that lead to challenges reproducing measured temperatures, but those uncertainties are likely a secondary factor in the error between RELAP5-3D and experimental data. The RELAP5-3D ring model of HTTF has been used in multiple analyses, but the work presented here suggests that the model's nodalization is insufficient to fully validate RELAP5-3D against HTTF, though we show that the model can reproduce trends in HTTF experiments quite well. These results are consistent with the previous HTTF analyses with RELAP5-3D and SAM. Based on the analyses in this paper, we were able to achieve only limited validation of RELAP5-3D for analysis of HTGR systems based on HTTF data. While this analysis could only partially reproduce HTTF temperatures, a more detailed model containing heat structures representing each azimuthal sector of the core and with a finer radial nodalization may be able to reproduce HTTF temperatures.

Acknowledgments

This research was funded by the U.S. Department of Energy Advanced Reactor Technologies Program for Gas Cooled Reactors (ART-GCR).

The authors would like to thank Mr. Paul Bayless for developing the RELAP5-3D ring model of HTTF that was used as the starting point for this analysis. We would also like to thank Dr. Paolo Balestra and Dr. Daniel Mikkelson for their thorough review of this manuscript draft.

This research made use of the resources of the High Performance Computing Center at INL, which is supported by the Office of Nuclear Energy of the U.S. Department of Energy and the Nuclear Science User Facilities under Contract No. DE-AC07-05ID14517.

References

Bayless, P., 2018. RELAP5-3D Input Model for the High Temperature Test Facility. Idaho Falls, ID (United States). https://doi.org/10.2172/1811538.

Bess, J.D., Dolphin, B.H., Core, F., 2010. Evaluation of the Start- Up Core Physics Tests at Japan ' s High Temperature Engineering Test Reactor (Fully- Loaded Core), International Handbook of Reactor Physics Experiments.

Bostelmann, F., Celik, C., Williams, M.L., Ellis, R.J., Ilas, G., Wieselquist, W.A., 2020. SCALE capabilities for high temperature gas-cooled reactor analysis. Ann. Nucl. Energy 147, 107673. https://doi.org/10.1016/j.anucene.2020.107673.

Bostelmann, F., Hammer, H.R., Ortensi, J., Strydom, G., Velkov, K., Zwermann, W., 2016. Criticality calculations of the Very High Temperature Reactor Critical Assembly benchmark with Serpent and SCALE/KENO-VI. Ann. Nucl. Energy 90, 343–352. https://doi.org/10.1016/j.anucene.2015.12.008.

Bostelmann, F., Strydom, G., 2017. Nuclear data uncertainty and sensitivity analysis of the VHTRC benchmark using SCALE. Ann. Nucl. Energy 110, 317–329. https://doi.org/10.1016/j.anucene.2017.06.052.

Cadell, S.R., Woods, B.G., 2019a. OSU High Temperature Test Facility Test Acceptance Report: PG-26 Low Power (<350 kW) Double Ended Inlet-Outlet Crossover Duct Break, 2 Heaters. Corvallis, OR.

Cadell, S.R., Woods, B.G., 2019b. OSU High Temperature Test Facility Test Acceptance Report: PG-27 Low Power (< 350 kW) Complete Loss of FLow, 2 Heaters. Corvallis, OR.

Duchnowski, E.M., Kile, R.F., Bott, K., Snead, L.L., Trelewicz, J.R., Brown, N.R., 2022. Pre-conceptual high temperature gas-cooled microreactor design utilizing two-phase composite moderators. Part I: Microreactor design and reactor performance. Prog. Nucl. Energy 149, 104257. https://doi.org/10.1016/j.pnucene.2022.104257.

Epiney, A., 2020. RELAP5-3D Modeling of High Temperature Test Facility (HTTF) Test PG-26. Idaho Falls, ID (United States). https://doi.org/10.2172/1676420.

Epiney, A., Hua, T., Wolf, J., Zou, L., Strydom, G., Hu, R., 2021. Modeling of HTTF test PG-26 using RELAP5-3D and SAM, in: Transactions of the American Nuclear Society. pp. 831–834. https://doi.org/10.13182/T124-35155.

Epiney, A., Strydom, G., Kile, R., Tano Retamales, M., Yoon, S., Mueller, C., Gutowska, I., Hua, T., Fang, J., Yuan, . H., Zou, L., Podila, K., Huang, X., Chen, Q., Jafri, T., Waddington, G., Pfeiffer, P., Li, C., 2022. OECD/NEA High Temperature Test Facility (HTTF) Thermal-Hydraulics Benchmark: Proposed Exercises, in: Transactions of the American Nuclear Society. Phoenix, AZ, USA.

Epiney, A.S., 2020. RELAP5-3D Modeling of High Temperature Test Facility Test PG-26. Idaho Falls, ID.

Fujimoto, N., Nojiri, N., Yamashita, K., 2004. Validation of the nuclear design code system for the HTTR using the criticality assembly VHTRC. Nucl. Eng. Des. 233, 155–162. https://doi.org/10.1016/j.nucengdes.2004.08.005.

Gairola, A., Epiney, A.S., 2021. RELAP5-3D Simulation of PG-27 Test at the HTTF. Idaho Falls, ID.

Gutowska, I., Woods, B., 2019a. OSU High Temperature Test Facility Design Technical Report, Revision 2. Corvallis, OR.

Gutowska, I., Woods, B., 2019b. Instrumentaion Plan for the OSU High Temperature Test

Facility. Corvallis, OR.
Halsted, J., Gutowska, I., 2023. Verification and validation of a lower plenum mixing test at the OSU High Temperature Test Facility. Nucl. Eng. Des. 406, 112251. https://doi.org/10.1016/j.nucengdes.2023.112251.
Japan Atomic Energy Research Institute, Gesselschaft fuer Anlagen-und Reaktorsicherheit, Siemens AG, U.K., United States Nuclear Regulatory Commission, MPR Assiciates Inc, 1993. International Agreement Report 2D / 3D Program Work Summary Report. Rockville, Maryland.
Kile, R.F., Epiney, A.S., Brown, N.R., 2023. High Temperature Test Facility sensitivity and calibration studies to inform OECD-NEA benchmark calculations. Nucl. Eng. Des. 404, 112178. https://doi.org/10.1016/j.nucengdes.2023.112178.
Martin, R.P., Place, R., Strydom, G., 2022. Datasets for RELAP5-3D HTGR Validation, in: The 19th International Topical MEeting on Nuclear Reactor Thermal Hydraulics (NURETH-19). pp. 1–16.
Meehan, N., Maldonado, G.I., Brown, N.R., 2022. Demonstration of RELAP5-3D for transient analysis of a dual coolant lead lithium fusion blanket concept. Fusion Eng. Des. 180, 113192. https://doi.org/10.1016/j.fusengdes.2022.113192.
Nakhnikian-Weintraub, B., Babineau, U., Woods, B.G., 2019. OSU High Temperature Test Facility Test Acceptance Report: PG-29 Low Power (<350 kw) Double Ended Inlet-Outlet Crossover Duct Break, Hybrid Heater. Corvallis, OR.
Ooi, Z.J., Hua, T., Zou, L., Hu, R., 2022. Simulation of the High Temperature Test Facility (HTTF) Core Using the 2D Ring Model with SAM. Nucl. Sci. Eng. 00, 1–28. https://doi.org/10.1080/00295639.2022.2106726.
Ortensi, J., Strydom, G., Sen, S., Seker, V., Ivanov, K., Clifford, I., Hou, J., Lee, H.C., Tak, N.-I., Han, T.-Y., Shim, H.J., Rhode, U., Fridman, E., Bilodid, Y., Seubert, A., 2017. NEA benchmark of the Modular High-Temperature Gas-Cooled Reactor-350 MW Core Design Volumes I and II.
Petti, D., Hill, R., Gehin, J., Gougar, H., Strydom, G., O'Connor, T., Heidet, F., Kinsey, J., Grandy, C., Qualls, A., Brown, N., Powers, J., Hoffman, E., Croson, D., 2017. A summary of the Department of Energy's advanced demonstration and test reactor options study. Nucl. Technol. 199, 111–128. https://doi.org/10.1080/00295450.2017.1336029.
Podila, K., Chen, Q., Huang, X., Li, C., Rao, Y., Waddington, G., Jafri, T., 2022. Coupled simulations for prismatic gas-cooled reactor. Nucl. Eng. Des. 395. https://doi.org/10.1016/j.nucengdes.2022.111858.
Rabiti, C., Alfonsi, A., Cogliati, J., Mandelli, D., Kinoshita, R., Sen, S., 2015. RAVEN User Manual.
Schultz, R.R., 1993. International agreement report international Code Assessment and Applications Program : Summary of Code Assessment Studies, NUREG/IA-0128.
Shin, D.-H., Yoon, S.-J., Tak, N.-I., Park, G.-C., Cho, H.-K., 2015. Analytical Study on the Effective Thermal Conductivity of VHTR Fuel Block Geometry with Multiple Cylindrical Holes. Nucl. Technol. 191, 213–222. https://doi.org/10.13182/NT14-102.
Stainsby, R., Grief, A., Worsley, W., Heerden, E., Dawson, F., Deniier, A., Bowman, W., 2009. Investigation of local heat transfer phenomena in a prismatic modular reactor core, NR001/RP/001.

Strydom, G., Epiney, A.S., Alfonsi, A., Rabiti, C., 2016. Comparison of the PHISICS/RELAP5-3D ring and block model results for phase I of the OECD/NEA MHTGR-350 benchmark. Nucl. Technol. 193, 15–35. https://doi.org/10.13182/NT14-146.
Takamatsu, K., Tochio, D., Nakagawa, S., Takada, S., Yan, X.L., Sawa, K., Sakaba, N., Kunitomi, K., 2014a. Experiments and validation analyses of HTTR on loss of forced cooling under 30% reactor power. J. Nucl. Sci. Technol. 51, 1427–1443. https://doi.org/10.1080/00223131.2014.967324
Takamatsu, K., Yan, X.L., Nakagawa, S., Sakaba, N., Kunitomi, K., 2014b. Spontaneous stabilization of HTGRs without reactor scram and core cooling - Safety demonstration tests using the HTTR: Loss of reactivity control and core cooling. Nucl. Eng. Des. 271, 379–387. https://doi.org/10.1016/j.nucengdes.2013.12.005.
The RELAP5-3D Code Development Team, 2018. RELAP5-3D Code Manual Volumes I-V.